In conclusion, we developed a new gene delivery system applicable to bone regenerative medicine. This polyplex nanomicelle showed high biocompatibility as well as a capacity for regulated gene transfer, inducing a remarkable increase in the bone regeneration rate in a bone defect model. This system holds much promise for constructing a practical gene-activated matrix for tissue engineering. Moreover, this technology will help realize therapeutic applications of gene therapy requiring safe and regulated gene expressions.

MATERIALS AND METHODS

Materials. pDNAs encoding luciferase (pGL3-control, 5,256bp) (Promega, Madison, WI) and GFP (pEGFP-C1, 4,700bp) (Clontech, Palo Alto, CA) were amplified in competent DH5α *Escherichia coli* and purified using EndoFree Plasmid Maxi or Mega Kits (Qiagen, Hilden, Germany). pCMV5 pDNA expressing hemagglutinin-tagged mouse caALK6 and pcDEF3 pDNA expressing Flag-tagged mouse Runx2 were generous gifts from M. Krüppel (Mt. Sinai Hospital, Toronto, Canada) and K. Miyazono (University of Tokyo, Tokyo, Japan), respectively. The DNA concentration was determined by reading the absorbance at 260nm. Commercially available transfection reagents, linear polyethylenimine (Exgen 500, M_w of LPEI = 22kd) and FuGENE6 were purchased from MBI Fermentas (Burlington, Canada) and Roche (Basel, Switzerland), respectively. Dulbecco's modified Eagle's medium and fetal bovine serum were purchased from Sigma-Aldrich (St. Louis, MO).

Synthesis and characterization of PEG-b-P[Asp-(DET)] block copolymer. The PEG-b-P[Asp-(DET)] block copolymer was synthesized as previously reported.[24] Briefly, PEG-poly(β-benzyl-L-aspartate) (PEG-PBLA) diblock copolymer was synthesized by the ring-opening polymerization of β-benzyl-L-aspartate *N*-carboxy-anhydride from the terminal primary amino group of α-methoxy-ω-amino PEG (M_w: 12,000; Nippon Oil and Fats, Tokyo, Japan). The copolymer thus prepared was confirmed to be unimodal with a narrow molecular weight distribution (M_w/M_n: 1.23) by gel-permeation chromatography, and the number of repeating units of BLA was calculated to be 68 by ^{1}H-NMR (data not shown). The N-terminal amino group of PEG-PBLA was then acetylated using acetic anhydride in dichloromethane solution to obtain PEG-PBLA-Ac. The obtained polymer was dissolved in distilled *N,N*-dimethylformamide (Wako Pure Chemical Industries, Osaka, Japan) and reacted with diethylenetriamine (DET) (Tokyo Kasei Kogyo, Tokyo, Japan) for 24 hours at 40°C under a dry argon atmosphere to undergo aminolysis of the benzyl side chain. After 24 hours, the solution was slowly dropped into 10% acetic acid solution and dialyzed (Spectra/por Membrane, molecular weight cut-off = 3,500, Rancho Dominquez, CA) against 0.01 N HCl and subsequently against distilled water. The final solution was lyophilized to obtain PEG-b-P[Asp-(DET)] as the hydrochloride salt form. ^{1}H-NMR confirmed the complete substitution of benzyl ester of the polymer with DET through the aminolysis reaction as well as the chemical structure of the obtained PEG-b-P[Asp-(DET)] block copolymer.

Preparation of pDNA carriers. The PEG-b-P[Asp-(DET)] block copolymer and pDNA were separately dissolved in 10mmol/l Tris-HCl buffer (pH 7.4). Both solutions were mixed at various nitrogen/phosphate (= (total amines in cationic segment)/(DNA phosphates)) and left overnight. The pDNA complexes with LPEI and FuGENE6 were prepared by mixing the pDNA solution and the reagents following the protocols provided by the manufacturers.

In vitro *transfection.* HEK293 cells were obtained from the Riken Cell Bank (Tsukuba, Japan). Mouse calvarial cells were isolated from calvariae of neonatal littermates. The experimental procedures were in accordance with the guidelines of the Animal Committee of the University of Tokyo. Calvariae were digested for 10 minutes at 37°C in an enzyme solution containing 0.1% collagenase and 0.2% dispase for five cycles. Cells isolated by the final four digestions were combined as an osteoblast population and cultured in Dulbecco's modified Eagle's medium containing 10% fetal bovine serum. Human synovial cells from rheumatoid arthritis patients were kindly provided by Dr. S. Tanaka (University of Tokyo).[46] Written informed consent for subsequent experiments was obtained from each patient.

For luciferase transfection assays, the cells were inoculated at a density of 2×10^4 cells/well in a 24-multiwell plate and cultured for 24 hours. After the culture medium was replaced with fresh medium containing 10% fetal bovine serum, pDNA carrier solution (33.3μg/ml, 22.5ml) was applied to each well. After several days of incubation, the cells were lysed and the luciferase gene expression was measured using a Luciferase Assay System (Promega, Madison, WI) and a Lumat LB9507 luminometer (Berthold, Bad Wildbad, Germany). The expression was normalized to protein concentrations of cell lysates. For the evaluation of sustained luciferase expression (**Figure 4**), the cells were seeded onto a 96-multiwell plate (6×10^3 cells/well). After incubation for 24 hours, 6μl of each pDNA carrier solution was added, followed by further incubation for up to day 10. The luminescence was measured by a GloMax 96 Microplate Luminometer (Promega, Madison, WI). For the GFP transfection assay, both the phase contrast and the fluorescence images were obtained by an Axiovert 100 M microscope (Carl Zeiss, Oberkochen, Germany).

For the cytotoxicity assay, a 96-multiwell plate was used. After transfection as described above, the cells were incubated for 2 or 5 days and their viability was evaluated by an MTT assay (Cell Counting Kit-8, Dojindo, Kumamoto, Japan). Each well was measured by reading the absorbance at 450nm according to the protocol provided by the manufacturer. The results were expressed as the relative value (%) of the control cells, which were incubated in parallel without transfection.

Evaluation of mRNA expression. After transfection to mouse calvarial cells, the total RNA was collected using the RNeasy Mini Preparation Kit (Qiagen, Hilden, Germany) according to the manufacturer's protocol. Gene expression was analyzed by quantitative PCR. Using the Quantitect SYBR Green PCR Kit (Qiagen, Hilden, Germany), 20ng of total RNA was analyzed in a final volume of 20μl according to the manufacturer's protocol. Reverse transcription was performed for 30 minutes at 50°C followed by PCR: 40 thermal cycles of 15 seconds at 94°C, 30 seconds at 55°C, and 30 seconds at 72°C using an ABI Prism 7500 Sequence Detector (Applied Biosystems, Foster City, CA). Each mRNA expression was normalized to levels of mouse β-actin mRNA, also determined by quantitative reverse transcription-PCR, from the same total RNA samples. The following primers were used: osteocalcin, forward primer (AAGCAGGAGGGC AATAAGGT) and reverse primer (TTTGTAGGCGGTCTTCAAGC); mouse ALK6, forward primer (CACCAAGAAGGAGGATGGAG) and reverse primer (CTAGACATCCAGAGGTGACAACAG); mouse Runx2, forward primer (CCCAGCCACCTTTACCTACA) and reverse primer (TATGGAGTGCTGCTGGTCTG); luciferase, forward primer (TTGA CCGCCTGAAGTCTCTGA) and reverse primer (ACACCTGCGTCGA AGATGTTG); mouse β-actin, forward primer (AGATGTGGATCAG CAAGCAG) and reverse primer (GCGCAAGTTAGGTTTTGTCA). As for luciferase, the gene expression presented as the light units was also evaluated in parallel.

In vitro *transfection from gene-containing scaffolds.* To prepare the scaffolds containing gene carriers, the PEG-P[Asp-(DET)]/pDNA micelles were mixed with calcium phosphate paste (BIOPEX-R; Mitsubishi Pharma, Osaka, Japan). According to the manufacturer's information, the powder consists of particles (2–5mm in diameter) of α-tricalcium phosphate (75% wt), tetracalcium phosphate monoxide (18% wt), dicalcium phosphate dibasic (5% wt), and hydroxyapatite (2% wt); the aqueous solution contains sodium chondroitin sulfate (5.4%) and sodium succinate

(13%). For solidification, 1.0 g of the powder was manually mixed (at low shear rates) with 233 μl of the solution containing pDNAs. After solidification, the cement containing 1.3 μg of pDNA was placed onto the upper chamber of a BD Falcon Cell Culture Insert for 12-well plates (1.0 μm pore size, Becton Dickinson, Franklin Lakes, NJ), and HEK293 cells were plated onto the lower chamber. Five days later, luciferase assay was performed as described. The level of luciferase expression was normalized to the protein concentrations of cell lysates.

In vivo *gene delivery for the bone defect area on the mouse skull bone.* In this study, the 4 mm defects in diameter were chosen as the mouse bone defect model.[47,48] We have observed that the mouse calvarial defects (4 mm in diameter) could not be covered spontaneously with regenerated bone within 8 weeks after operation, although significant bone formation was observed at the defect edge (data not shown). Thus, the bone regeneration was evaluated within or at 4 weeks after gene delivery.

For the generation of bone defects, mice were anesthetized with ketamine/xylazine (80 mg/kg and 5 mg/kg) solution through intraperitoneal injection, and a linear incision was made along the sagittal suture from the frontal bone to the center of the occipital bone. A round craniotomy defect (4 mm in diameter) was manually created on both parietal bones with a sterile disposable trephine (Kai Industries, Gifu, Japan).[47] Calcium phosphate paste was used to fill in the defects, and then the incisions were sutured. The mice were killed at 2, 4, or 8 weeks after the operation for radiologic, histologic, or immunohistologic analyses, respectively. Animal experiments were performed according to the protocol approved by the Animal Care and Use Committee of the University of Tokyo.

Assessment of bone regeneration. After the mice were asphyxiated with carbon dioxide, the calvarias were removed. Tissue preparation, hematoxylin and eosin staining, and immunohistologic analysis using a rabbit polyclonal antibody against GFP (Molecular Probes, Eugene, OR) or a rabbit polyclonal antibody against type-I collagen (LSL, Tokyo, Japan) were performed as described.[49] To evaluate the extent of bone regeneration, serial coronal sections of the implantation site were performed at 0.5, 1, 1.5, 2, 2.5, 3, and 3.5 mm from the rostral end and then stained with hematoxylin and eosin. For each section, the original defect area and the regenerated bone area were measured by NIH Image software. The ratio of the summation of the regenerated bone area to that of the original defect area (SRBA/SODA) was calculated and used as the index of bone regeneration.

ACKNOWLEDGMENTS

We thank Michael Klüppel (Mount Sinai Hospital) and Kohei Miyazono (University of Tokyo) for pDNAs expressing caALK6 and Runx2, respectively. We also appreciate Sakae Tanaka (University of Tokyo) for providing human synovial cells. This work was supported by Grants-in-Aid for Scientific Research from the Japanese Ministry of Education, Culture, Sports, Science and Technology (#15390452 and #17390530), Health Science Research Grants from the Japanese Ministry of Health, Labor and Welfare (#H16-regenerative medicine-008), and the Core Research Program for Evolutional Science and Technology (CREST) from the Japan Science and Technology Corporation (JST).

SUPPLEMENTARY MATERIAL

Figure S1. Zeta-potential of polyplex nanomicelles and pDNA complexes with P[Asp-(DET)], the cationic segment of the block copolymer used in this study.

Figure S2. GFP gene expression in human synovial cells.

Figure S3. GFP gene expression in mouse calvarial cells.

Figure S4. *In vitro* transfection by polyplex nanomicelles incorporated into calcium phosphate cement scaffold.

REFERENCES

1. Bucholz, RW, Heckman, JD (2006). *Rockwood and Green's Fractures in Adults*. Lippincott Williams & Wilkins: Philadelphia, PA. 587pp.
2. Banwart, JC, Asher, MA and Hassanein, RS (1995). Iliac crest bone graft harvest donor site morbidity. A statistical evaluation. *Spine* **20**: 1055–1060.
3. Arrington, ED, Smith, WJ, Chambers, HG, Bucknell, AL and Davino, NA (1996). Complications of iliac crest bone graft harvesting. *Clin Orthop Relat Res* **329**: 300–309.
4. Langer, R and Vacanti, JP (1993). Tissue engineering. *Science* **260**: 920–926.
5. Bruder, SP and Caplan, AI (2000). *Principles of Tissue Engineering*. Academic Press: San Diego, CA. 683pp.
6. Winn, SR, Hu, Y, Sfeir, C and Hollinger, JO (2000). Gene therapy approaches for modulating bone regeneration. *Adv Drug Deliv Rev* **42**: 121–138.
7. Baltzer, AW and Lieberman, JR (2004). Regional gene therapy to enhance bone repair. *Gene Ther* **11**: 344–350.
8. Katagiri, T and Takahashi, N (2002). Regulatory mechanisms of osteoblast and osteoclast differentiation. *Oral Dis* **8**: 147–159.
9. Long, F, Chung, UI, Ohba, S, McMahon, J, Kronenberg, HM and McMahon, AP (2004). Ihh signaling is directly required for the osteoblast lineage in the endochondral skeleton. *Development* **131**: 1309–1318.
10. Komori, T (2003). Requisite roles of Runx2 and Cbfb in skeletal development. *J Bone Miner Metab* **21**: 193–197.
11. Patel, MS and Karsenty, G (2002). Regulation of bone formation and vision by LRP5. *N Engl J Med* **346**: 1572–1574.
12. Ogata, N, Chikazu, D, Kubota, N, Terauchi, Y, Tobe, K, Azuma, Y *et al.* (2000). Insulin receptor substrate-1 in osteoblast is indispensable for maintaining bone turnover. *J Clin Invest* **105**: 935–943.
13. Govender, S, Csimma, C, Genant, HK, Valentin-Opran, A, Amit, Y, Arbel, R *et al.* (2002). Recombinant human bone morphogenetic protein-2 for treatment of open tibial fractures: a prospective, controlled, randomized study of four hundred and fifty patients. *J Bone Joint Surg Am* **84-A**: 2123–2134.
14. Valentin-Opran, A, Wozney, J, Csimma, C, Lilly, L and Riedel, GE (2002). Clinical evaluation of recombinant human bone morphogenetic protein-2. *Clin Orthop Relat Res* **395**: 110–120.
15. Gerstenfeld, LC, Cullinane, DM, Barnes, GL, Graves, DT and Einhorn, TA (2003). Fracture healing as a post-natal developmental process: molecular, spatial, and temporal aspects of its regulation. *J Cell Biochem* **88**: 873–884.
16. Howell, TH, Fiorellini, J, Jones, A, Alder, M, Nummikoski, P, Lazaro, M *et al.* (1997). A feasibility study evaluating rhBMP-2/absorbable collagen sponge device for local alveolar ridge preservation or augmentation. *Int J Periodontics Restorative Dent* **17**: 124–139.
17. Zhao, M, Zhao, Z, Koh, JT, Jin, T and Franceschi, RT (2005). Combinatorial gene therapy for bone regeneration: cooperative interactions between adenovirus vectors expressing bone morphogenetic proteins 2, 4, and 7. *J Cell Biochem* **95**: 1–16.
18. Riew, KD, Wright, NM, Cheng, S, Avioli, LV and Lou, J (1998). Induction of bone formation using a recombinant adenoviral vector carrying the human BMP-2 gene in a rabbit spinal fusion model. *Calcif Tissue Int* **63**: 357–360.
19. Rutherford, RB, Moalli, M, Franceschi, RT, Wang, D, Gu, K and Krebsbach, PH (2002). Bone morphogenetic protein-transduced human fibroblasts convert to osteoblasts and form bone *in vivo*. *Tissue Eng* **8**: 441–452.
20. Schek, RM, Hollister, SJ and Krebsbach, PH (2004). Delivery and protection of adenoviruses using biocompatible hydrogels for localized gene therapy. *Mol Ther* **9**, 130–138.
21. Gafni, Y, Pelled, G, Zilberman, Y, Turgeman, G, Apparailly, F, Yotvat, H *et al.* (2004). Gene therapy platform for bone regeneration using an exogenously regulated, AAV-2-based gene expression system. *Mol Ther* **9**: 587–595.
22. Lundstrom, K (2003). Latest development in viral vectors for gene therapy. *Trends Biotechnol* **21**: 117–122.
23. Egermann, M, Lill, CA, Griesbeck, K, Evans, CH, Robbins, PD, Schneider, E *et al.* (2006). Effect of BMP-2 gene transfer on bone healing in sheep. *Gene Ther* **13**: 1290–1299.
24. Kanayama, N, Fukushima, S, Nishiyama, N, Itaka, K, Jang, WD, Miyata, K *et al.* (2006). A PEG-based biocompatible block catiomer with high buffering capacity for the construction of polyplex micelles showing efficient gene transfer toward primary cells. *ChemMedChem* **1**: 439–444.
25. Harada-Shiba, M, Yamauchi, K, Harada, A, Takamisawa, I, Shimokado, K and Kataoka, K (2002). Polyion complex micelles as vectors in gene therapy—pharmacokinetics and *in vivo* gene transfer. *Gene Ther* **9**: 407–414.
26. Itaka, K, Harada, A, Nakamura, K, Kawaguchi, H and Kataoka, K (2002). Evaluation by fluorescence resonance energy transfer of the stability of nonviral gene delivery vectors under physiological conditions. *Biomacromolecules* **3**: 841–845.
27. Itaka, K, Yamauchi, K, Harada, A, Nakamura, K, Kawaguchi, H and Kataoka, K (2003). Polyion complex micelles from plasmid DNA and poly(ethylene glycol)-poly(L-lysine) block copolymer as serum-tolerable polyplex system: physicochemical properties of micelles relevant to gene transfection efficiency. *Biomaterials* **24**: 4495–4506.
28. Boussif, O, Lezoualc'h, F, Zanta, MA, Mergny, MD, Scherman, D, Demeneix, B *et al.* (1995). A versatile vector for gene and oligonucleotide transfer into cells in culture and *in vivo*: polyethylenimine. *Proc Natl Acad Sci USA* **92**: 7297–7301.
29. Hellgren, I, Drvota, V, Pieper, R, Enoksson, S, Blomberg, P, Islam, KB *et al.* (2000). Highly efficient cell-mediated gene transfer using non-viral vectors and FuGene6: *in vitro* and *in vivo* studies. *Cell Mol Life Sci* **57**: 1326–1333.
30. Weiskirchen, R, Kneifel, J, Weiskirchen, S, van de Leur, E, Kunz, D and Gressner, AM (2000). Comparative evaluation of gene delivery devices in primary cultures of rat hepatic stellate cells and rat myofibroblasts. *BMC Cell Biol* **1**: 4.
31. Lee, MJ, Cho, SS, You, JR, Lee, Y, Kang, BD, Choi, JS *et al.* (2002). Intraperitoneal gene delivery mediated by a novel cationic liposome in a peritoneal disseminated ovarian cancer model. *Gene Ther* **9**: 859–866.
32. Elmadbouh, I, Rossignol, P, Meilhac, O, Vranckx, R, Pichon, C, Pouzet, B *et al.* (2004). Optimization of *in vitro* vascular cell transfection with non-viral vectors for *in vivo* applications. *J Gene Med* **6**: 1112–1124.
33. Tinsley, RB, Faljerson, J and Eriksson, PS (2006). Efficient non-viral transfection of adult neural stem/progenitor cells, without affecting viability, proliferation or differentiation. *J Gene Med* **8**: 72–81.
34. Ohba, S, Ikeda, T, Kugimiya, F, Yano, F, Lichtler, AC, Nakamura, K *et al.* (2007). Identification of a potent combination of osteogenic genes for bone

regeneration using embryonic stem (ES) cell-based sensor. *FASEB J* (epub ahead of print).
35. Hunter, AC (2006). Molecular hurdles in polyfectin design and mechanistic background to polycation induced cytotoxicity. *Adv Drug Deliv Rev* **58**: 1523–1531.
36. Bonadio, J, Smiley, E, Patil, P and Goldstein, S (1999). Localized, direct plasmid gene delivery *in vivo*: prolonged therapy results in reproducible tissue regeneration. *Nat Med* **5**: 753–759.
37. Verma, IM and Somia, N (1997). Gene therapy—promises, problems and prospects. *Nature* **389**: 239–242.
38. Bright, C, Park, YS, Sieber, AN, Kostuik, JP and Leong, KW (2006). *In vivo* evaluation of plasmid DNA encoding OP-1 protein for spine fusion. *Spine* **31**: 2163–2172.
39. Huang, YC, Simmons, C, Kaigler, D, Rice, KG and Mooney, DJ (2005). Bone regeneration in a rat cranial defect with delivery of PEI-condensed plasmid DNA encoding for bone morphogenetic protein-4 (BMP-4). *Gene Ther* **12**: 418–426.
40. Moghimi, SM, Symonds, P, Murray, JC, Hunter, AC, Debska, G and Szewczyk, A (2005). A two-stage poly(ethylenimine)-mediated cytotoxicity: implications for gene transfer/therapy. *Mol Ther* **11**: 990–995.
41. Geiger, F, Bertram, H, Berger, I, Lorenz, H, Wall, O, Eckhardt, C *et al.* (2005). Vascular endothelial growth factor gene-activated matrix (VEGF165-GAM) enhances osteogenesis and angiogenesis in large segmental bone defects. *J Bone Miner Res* **20**: 2028–2035.
42. Omidi, Y, Hollins, AJ, Benboubetra, M, Drayton, R, Benter, IF and Akhtar, S (2003). Toxicogenomics of non-viral vectors for gene therapy: a microarray study of lipofectin- and oligofectamine-induced gene expression changes in human epithelial cells. *J Drug Target* **11**: 311–323.
43. Kabanov, AV, Batrakova, EV, Sriadibhatla, S, Yang, Z, Kelly, DL and Alakov, VY (2005). Polymer genomics: shifting the gene and drug delivery paradigms. *J Control Release* **101**: 259–271.
44 Buttery, LD, Bourne, S, Xynos, JD, Wood, H, Hughes, FJ, Hughes, SP *et al.* (2001). Differentiation of osteoblasts and *in vitro* bone formation from murine embryonic stem cells. *Tissue Eng* **7**: 89–99.
45. Jiang, Y, Vaessen, B, Lenvik, T, Blackstad, M, Reyes, M and Verfaillie, CM (2002). Multipotent progenitor cells can be isolated from postnatal murine bone marrow, muscle, and brain. *Exp Hematol* **30**: 896–904.
46. Seto, H, Kamekura, S, Miura, T, Yamamoto, A, Chikuda, H, Ogata, T *et al.* (2004). Distinct roles of Smad pathways and p38 pathways in cartilage-specific gene expression in synovial fibroblasts. *J Clin Invest* **113**: 718–726.
47. Hirata, K, Tsukazaki, T, Kadowaki, A, Furukawa, K, Shibata, Y, Moriishi, T *et al.* (2003). Transplantation of skin fibroblasts expressing BMP-2 promotes bone repair more effectively than those expressing Runx2. *Bone* **32**: 502–512.
48. Cowan, CM, Shi, YY, Aalami, OO, Chou, YF, Mari, C, Thomas, R *et al.* (2004). Adipose-derived adult stromal cells heal critical-size mouse calvarial defects. *Nat Biotechnol* **22**: 560–567.
49. Kugimiya, F, Kawaguchi, H, Kamekura, S, Chikuda, H, Ohba, S, Yano, F *et al.* (2005). Involvement of endogenous bone morphogenetic protein (BMP) 2 and BMP6 in bone formation. *J Biol Chem* **280**: 35704–35712.

ARTHRITIS & RHEUMATISM
Vol. 56, No. 10, October 2007, pp 3358–3365
DOI 10.1002/art.22941

Prevention of Cartilage Destruction With Intraarticular Osteoclastogenesis Inhibitory Factor/Osteoprotegerin in a Murine Model of Osteoarthritis

Sadanori Shimizu,[1] Yoshinori Asou,[1] Soichiro Itoh,[1] Ung-il Chung,[2] Hiroshi Kawaguchi,[2] Kenichi Shinomiya,[1] and Takeshi Muneta[1]

Objective. **To investigate the effect of osteoclastogenesis inhibitory factor/osteoprotegerin (OPG) on chondrocytes in the development of osteoarthritis (OA) in vivo.**

Methods. **To determine the role of endogenous OPG in the progression of OA, OA was surgically induced in $OPG^{+/-}$ mice and their wild-type (WT) littermates. To determine the role of exogenous OPG, knee joints of C57BL/6J mice with surgically induced OA were injected intraarticularly with recombinant human OPG (rHuOPG) or vehicle 5 times a week. All mice were euthanized 4 weeks after OA induction; joints were harvested and evaluated immunohistochemically.**

Results. **Although OA changes were induced in both WT and $OPG^{+/-}$ mice, the degenerative changes in the articular cartilage were significantly enhanced in $OPG^{+/-}$ mice. In C57BL/6J mice with surgically induced OA, intraarticular OPG administration protected the articular cartilage from the progression of OA. The Mankin and cartilage destruction scores in OPG-treated animals were ~50% of those seen in the control group. Furthermore, OPG administration significantly protected articular cartilage thickness. Findings of the TUNEL assay indicated that rHuOPG prevented chondrocyte apoptosis in joints with surgically induced OA. Results of immunostaining indicated that OPG protein was detected in the synovium and in resident chondrocytes at higher levels in the OPG-treated group than in the control group.**

Conclusion. **These data indicate that endogenous OPG had a protective effect against the cartilage destruction that occurs during OA progression. Furthermore, direct administration of rHuOPG to articular chondrocytes prevented cartilage destruction in an experimental murine model of OA via prevention of chondrocyte apoptosis.**

Osteoarthritis (OA), a chronic degenerative joint disorder characterized by articular cartilage destruction and osteophyte formation, is a major cause of disability worldwide (1). OA risk factors identified by previous epidemiologic studies are age, history of trauma, occupation, and sex. Since these factors are closely related to the mechanical load placed on joints, OA is thought to be induced primarily by accumulated mechanical stress (2). Although several symptomatic therapies have been attempted for OA, no radical treatment methods have been established, with the exception of arthroplasty. In OA, articular chondrocytes appear to be eliminated by apoptosis (2,3). The number of apoptotic cells in the articular cartilage of OA patients was found to be significantly higher than the number in healthy subjects (4). In addition, chondrocyte apoptosis has been reproduced in animals with experimentally induced OA (5).

Osteoclastogenesis inhibitory factor/osteoprotegerin (OPG) is a heparin-binding basic glycoprotein that was originally purified from the conditioned medium of the human embryonic lung fibroblast line IMR-90 (6). OPG is a secreted member of the tumor

Supported by Daiichi Sankyo Co., Ltd. Drs. Shimizu, Shinomiya, and Muneta's work was supported by the Center of Excellence Program for Frontier Research on Molecular Destruction and Reconstruction of Tooth and Bone, Tokyo Medical and Dental University.

[1]Sadanori Shimizu, MD, Yoshinori Asou, MD, PhD, Soichiro Itoh, MD, PhD, Kenichi Shinomiya, MD, PhD, Takeshi Muneta, MD, PhD: Tokyo Medical and Dental University, Tokyo, Japan; [2]Ung-il Chung, MD, PhD, Hiroshi Kawaguchi, MD, PhD: University of Tokyo, Tokyo, Japan.

Dr. Asou is submitting a patent application for an adaptation of osteoprotegerin.

Address correspondence and reprint requests to Yoshinori Asou, MD, PhD, Tokyo Medical and Dental University, Department of Orthopedic Surgery, 1-5-45 Yushima, Bunkyo-ku, Tokyo 113-8519, Japan. E-mail: aso.orth@tmd.ac.jp.

Submitted for publication January 8, 2007; accepted in revised form June 29, 2007.

necrosis factor (TNF) receptor family that functions as a decoy receptor for RANKL (6–8), serving to inhibit osteoclastogenesis and accelerate osteoclast apoptosis (9,10). OPG deficiency in mice causes severe bone loss and destruction of internal bone structures through an unbalanced shift in favor of osteoclast differentiation, but without other abnormalities (11–13). Homozygous OPG knockout ($OPG^{-/-}$) mice also exhibit unusual bone formations associated with severe destruction of growth plate cartilage (14,15). The proximal epiphyses of the femurs and humeri in $OPG^{-/-}$ mice exhibit resorption of subchondral bone and collapse of the joint surface resulting from mechanical damage at the end of the bone (13). Inactivating mutations in *TNFRSF11B*, the gene that encodes OPG, result in juvenile Paget's disease (16). Polymorphisms in OPG also increase the risk of developing Paget's disease (16). Patients with Paget's disease exhibit a wide range of clinical manifestations, including bone pain, fracture, hearing loss, syndromes of neurologic compression, and secondary OA (17).

RANK, RANKL, and OPG messenger RNA (mRNA) and proteins are expressed in normal cartilage. Cartilage from patients with OA contains increased levels of OPG mRNA, and the expression of these 3 proteins extends into the midzone of the cartilage (18,19). OPG is expressed in the synovial tissues of patients with rheumatoid arthritis, spondylarthropathies, and OA (19). OPG expression by chondrocytes is increased in response to in vitro stimulation with interleukin-1β, the proinflammatory cytokine expressed in OA joints (18), implying the existence of OPG targets within the joint space, in addition to the subchondral area.

The function of OPG that is expressed during OA pathogenesis is poorly understood. In this study, we investigated the effects of OPG on chondrocytes during OA development in vivo. We demonstrated that endogenous OPG functions in the prevention of articular cartilage degradation in a mechanical stress–induced animal model of OA. Furthermore, we found that direct administration of exogenous OPG to articular chondrocytes effectively retarded the progression of OA via suppression of chondrocyte apoptosis.

MATERIALS AND METHODS

Animals. C57BL/6J mice (8–10 weeks old) were purchased from Sankyo Labo (Tokyo, Japan). Mice heterozygous for the OPG gene mutation, OPG/Jcl, on a C57BL/6J background were purchased from Japan Clea (Tokyo, Japan).

Surgical induction of OA. All experiments were performed according to a protocol approved by the Animal Care and Use Committee of Tokyo Medical and Dental University. With the mice under general anesthesia, the right knee joint was surgically exposed. The medial collateral ligament was transected, and the medial meniscus was removed using a surgical microscope with microsurgical technique, as previously reported (1). The left knee joint was sham-operated, without ligament transection or meniscectomy.

Reagents. Recombinant human OPG (rHuOPG) was kindly provided by Biological Research Laboratories, Daiichi Sankyo (Tokyo, Japan).

Experimental design. *Surgical induction of OA in $OPG^{+/-}$ mice.* $OPG^{+/-}$ mice (n = 7) and their wild-type (WT) littermates (n = 7) (ages 8–12 weeks) were surgically induced to develop OA by medial collateral ligament transection and medial meniscectomy. Four weeks after surgery, the mice were euthanized.

Intraarticular administration of rHuOPG. After surgical induction of OA, C57BL/6J mice (n = 14) were divided into 2 groups. The OPG-treated group (n = 7) was administered 100 ng of rHuOPG in 10 μl of phosphate buffered saline (PBS) intraarticularly 5 days a week beginning on postoperative day 1 and continuing for 4 weeks after the operation. The control group (n = 7) received 10 μl of PBS intraarticularly according to the same schedule as in the OPG-treated group. Four weeks after surgery, the animals were euthanized.

Assessment of the severity of OA. Whole knee joints were removed by dissection, fixed in 4% paraformaldehyde, and decalcified in EDTA. After dehydration and paraffin embedding, we cut serial 5-μm sagittal sections from the whole medial compartment of the joint. Two sections obtained at 100-μm intervals from the weight-bearing region of each knee joint were stained with Safranin O–fast green. OA severity in the tibial plateau was evaluated according to Mankin's histologic grading system (20,21), and a cartilage destruction score was also assigned (1). The thickness of the articular cartilage layer was measured as the average distance from the superficial layer to the osteochondral junction of the tibia. Quantitative determination of the articular cartilage thickness and bone volume in subchondral bone was made using Image-Pro Plus 4.1 software (Media Cybernetics, Carlsbad, CA).

Immunohistochemical analysis. Expression of OPG and TRAIL at the protein level was examined by immunohistochemistry using an anti-mouse OPG antibody (N-20; catalog no. sc-8468) or an anti-mouse TRAIL antibody (K-18; catalog no. sc-6079) according to the manufacturer's instructions (Santa Cruz Biotechnology, Santa Cruz, CA). Briefly, sections were blocked with 5% normal rabbit serum for 30 minutes, then incubated overnight with anti-mouse OPG antibody (1:100 dilution) or with anti-mouse TRAIL antibody (1:20 dilution) at 4°C in a humidified chamber. Sections were incubated for 30 minutes at room temperature with a biotinylated rabbit anti-goat IgG and visualized by peroxidase-conjugated avidin and diaminobenzidine using a Vectastain kit (Vector, Burlingame, CA).

TUNEL assay. The TUNEL assay was performed using a TUNEL detection kit according to the manufacturer's instructions (Takara Shuzo, Kyoto, Japan). Briefly, sections were incubated with 15 μg/ml of proteinase K for 15 minutes at room temperature, then washed with PBS. Endogenous peroxidase was inactivated with 3% H_2O_2 for 5 minutes at room temperature. After washing with PBS, sections were immersed

in buffer containing deoxynucleotidyl transferase and biotinylated dUTP and incubated for 90 minutes at 37°C in a humid atmosphere. After washing in PBS, signals were examined by fluorescence microscopy.

Statistical analysis. Data are expressed as the mean ± SD. Statistical analysis was performed with the Mann-Whitney U test. P values less than 0.05 were considered significant.

RESULTS

Enhancement of cartilage destruction by OPG heterozygous deficiency in an experimental OA model. To determine the role of endogenous OPG in the progression of OA, we compared histologic features in the knee joints of OPG-deficient mice with those in their WT littermates. Histologic sections of the knee joints of young adult homozygous OPG-knockout ($OPG^{-/-}$) mice (8 weeks old) exhibited significantly thinned articular cartilage layers, active infiltration of vessels into subchondral bone, and irregularity of the osteochondral junction as compared with knee joints from $OPG^{+/-}$ mice and WT littermates (Figures 1A–C). With aging, cartilage degradation was found to be enhanced in $OPG^{-/-}$ mice and even in $OPG^{+/-}$ mice (Figures 1D–F), which suggests that sufficient levels of OPG expression are essential for the prevention of age-dependent cartilage degradation. However, it was unclear whether OPG affected chondrocyte metabolism directly or whether it was affected indirectly through osteoclastic erosion of subchondral bone via RANK signaling, since subchondral bone was apparently reduced in $OPG^{-/-}$ mice.

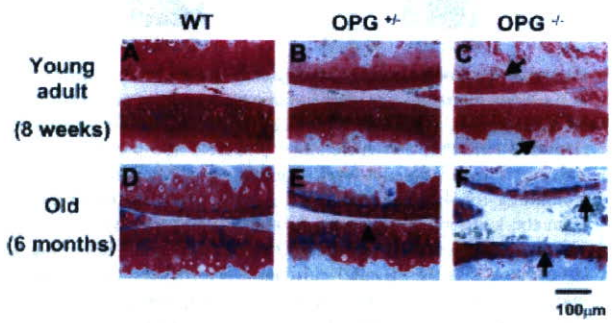

Figure 1. Histologic findings in the knee joints of young adult (8-week-old) and old (6-month-old) osteoprotegerin (OPG)–deficient mice and their wild-type (WT) littermates. Compared with the $OPG^{+/-}$ (**B**) and WT (**A**) littermates at 8 weeks of age, the $OPG^{-/-}$ mice (**C**) exhibited thinning of the articular cartilage layers, active infiltration of vessels into subchondral bone (**arrows**), and irregularity of the osteochondral junction. At 6 months of age, signs of enhanced cartilage degradation were observed in the OPG-deficient mice, such as superficial fibrillation (**E**) (**arrowhead**) and proteoglycan defects (**F**) (**arrows**), as compared with their WT littermates (**D**).

Therefore, we used young adult $OPG^{+/-}$ mice in our experimental model of OA to avoid the effect of the subchondral bone defect and to examine the effects of OPG insufficiency on cartilage.

We compared the rates of progression and the severity of OA in $OPG^{+/-}$ mice subjected to medial collateral ligament transection and medial meniscectomy to induce OA (1) with those in their WT littermates. Both the structure of the articular cartilage and the total bone volume were similar in $OPG^{+/-}$ mice and WT littermates at the ages examined (8–12 weeks old). Mice were euthanized 4 weeks after the operation, and the knee joints were harvested and evaluated histologically.

Destruction of the medial tibial cartilage was observed in WT littermates, as reported previously (1) (Figure 2A, parts a and c). Histologic evaluation revealed that degenerative changes of the articular cartilage were enhanced in $OPG^{+/-}$ mice as compared with WT littermates (Figure 2A, parts b and d). Both the Mankin scores (Figure 2B) and the cartilage destruction scores (Figure 2C) in $OPG^{+/-}$ mice were 25% higher than those in the WT littermates ($P < 0.05$). The morphology of subchondral bone structures was not affected by OPG haploinsufficiency (Figure 2A, parts c and d). Cartilage thickness, however, was significantly reduced ($P < 0.05$) in $OPG^{+/-}$ mice (Figure 2D), indicating that endogenous OPG plays an important role in the maintenance of articular cartilage during the development of mechanical stress–induced OA.

Prevention of cartilage destruction in an experimental OA model by exogenous OPG administration. To examine whether exogenous OPG prevents cartilage destruction independently of the protection of subchondral bone structures, we administered rHuOPG by intraarticular injection to induce OA surgically in C57BL/6J mice. We chose this method because systemic administration of OPG may affect subchondral bone metabolism via the suppression of osteoclastogenesis. Medial collateral ligament transection and medial meniscectomy to induce OA were performed on the right knees of all mice; sham operations were performed on the left knees. OPG or vehicle alone was injected intraarticularly 5 days a week beginning the day after the operation, and all mice were euthanized 4 weeks after the operation.

Histologic investigation indicated that OPG administration protected the articular cartilage from proteoglycan depletion, alterations of surface structure, and

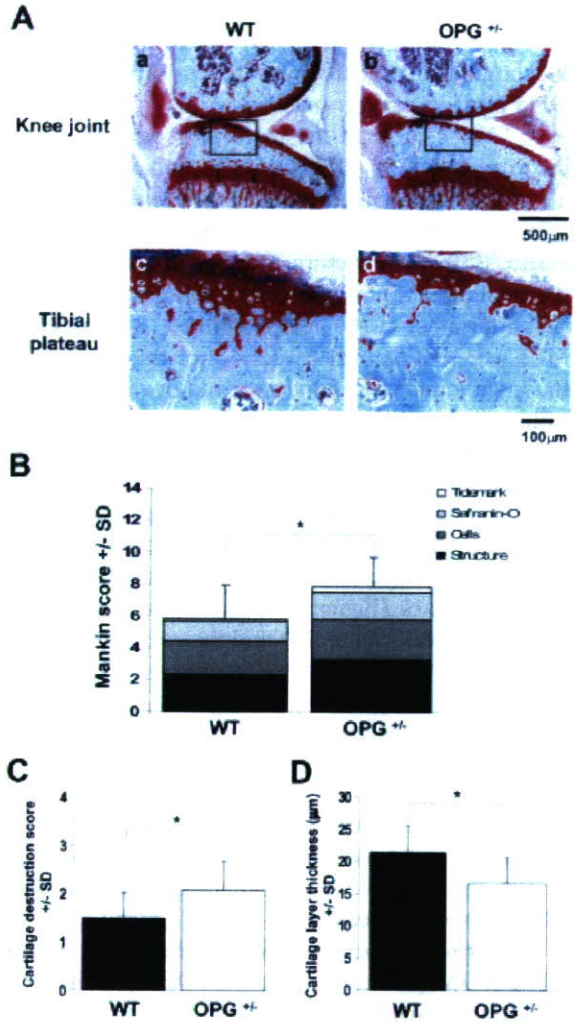

Figure 2. Histologic analysis of surgically induced osteoarthritis (OA) in the knee joints of young adult osteoprotegerin (OPG)–deficient mice and their wild-type (WT) littermates. OA was surgically induced in mice ages 8–12 weeks, and knee joints were harvested 4 weeks later. **A,** Sections of articular cartilage from WT (**a** and **c**) and $OPG^{+/-}$ (**b** and **d**) mice were stained with Safranin O to detect proteoglycans. Degenerative changes in the articular cartilage were enhanced in $OPG^{+/-}$ mice (**b**) as compared with their WT littermates (**a**). Morphologic features of the subchondral bone were similar in the WT (**c**) and $OPG^{+/-}$ (**d**) mice. Boxed and labeled areas in **a** and **b** are shown at higher magnification in **c** and **d**, respectively. **B** and **C,** Histologic changes in the OA joints were assigned Mankin scores (**B**) and cartilage destruction scores (**C**). Scores in the $OPG^{+/-}$ mice were 25% higher than those in their WT littermates. **D,** Mean cartilage thickness in OA joints was measured as the average distance from the superficial layer to the osteochondral junction of the tibia. The mean cartilage thickness was significantly reduced in $OPG^{+/-}$ mice as compared with their WT littermates. Values in **B–D** are the mean and SD of 7 mice per group. * = $P < 0.05$ by Mann-Whitney U test.

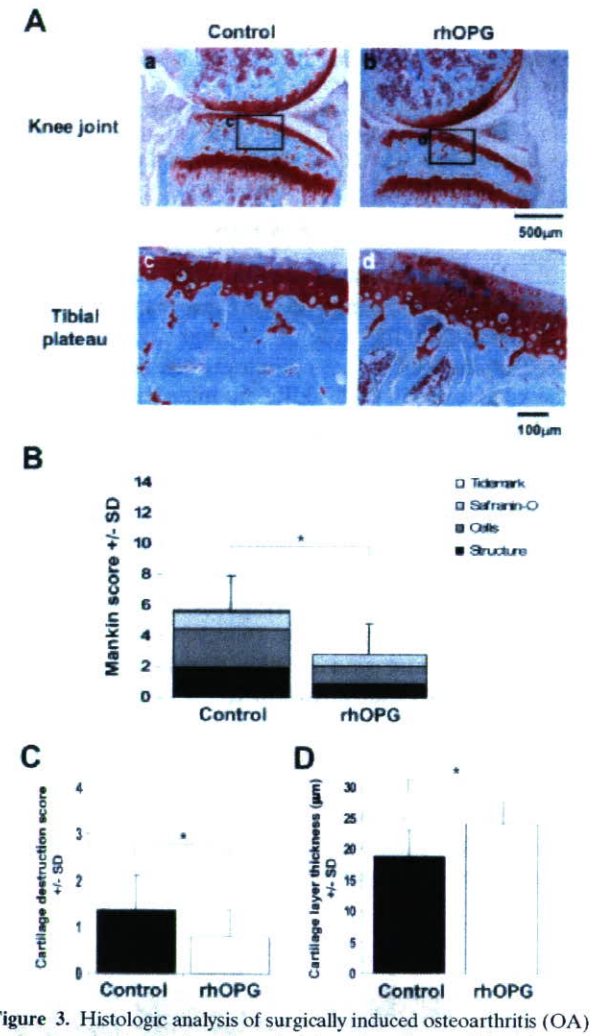

Figure 3. Histologic analysis of surgically induced osteoarthritis (OA) in the knee joints of mice after administration of recombinant human osteoprotegerin (rHuOPG) or vehicle. Intraarticular injection of rHuOPG (rhOPG) or vehicle alone (control) into mouse knee joints was performed 5 times a week beginning the day after surgery and continuing for 4 weeks thereafter. **A,** Sections of articular cartilage from the knee joints of control (**a** and **c**) or OPG-treated (**b** and **d**) mice were stained with Safranin O to detect proteoglycans. Degenerative changes in the articular cartilage were reduced in OPG-treated mice as compared with the controls (**a–d**). Morphologic features of the subchondral bone were similar in the control (**c**) and OPG-treated (**d**) mice. Boxed and labeled areas in **a** and **b** are shown at higher magnification in **c** and **d**, respectively. **B** and **C,** Histologic changes in the OA joints were assigned Mankin scores (**B**) and cartilage destruction scores (**C**). Scores in the OPG-treated mice were less than 50% of those in the controls. **D,** Mean cartilage thickness in OA joints was measured as the average distance from the superficial layer to the osteochondral junction of the tibia. The mean cartilage thickness was significantly reduced in the OPG-treated group as compared with the controls. Values in **B–D** are the mean and SD of 7 mice per group. * = $P < 0.05$ by Mann-Whitney U test.

clustering of chondrocytes (Figure 3A, parts a–d). At this time point, Mankin scores (Figure 3B) and cartilage destruction scores (Figure 3C) in OPG-treated animals were ~50% of those seen in the control group ($P < 0.05$). Thus, OPG administration significantly protected the articular cartilage thickness (Figure 3D). The structure and bone volume (mean ± SD bone volume/total volume 56.79 ± 12% in the control group versus 59.18 ± 22% in the OPG-treated group) of subchondral bone were not affected by intraarticular administration of OPG, as was expected (Figure 3A, parts c and d). The number of osteoclasts in the subchondral region (mean ± SD 4.4 ± 1.1/mm in the control group versus 4.4 ± 1.2/mm in the OPG-treated group) was also similar between these groups, indicating that exogenous OPG protected the articular cartilage from degradation in a manner that was independent of the protection of subchondral bone.

Prevention of chondrocyte apoptosis in an experimental OA model by exogenous OPG administration. Chondrocyte apoptosis is increased in OA cartilage and is anatomically linked to proteoglycan depletion (2,3). These observations prompted us to investigate the effect of OPG administration on chondrocyte apoptosis. We injected rHuOPG or vehicle alone into the knee joints of C57BL/6J mice with surgically induced OA for 5 days a week beginning on postoperative day 1 and continuing for 4 weeks. Knee joints were then examined after TUNEL staining. TUNEL-positive cells were abundant among the chondrocytes present in control mice with surgically induced OA that had received only PBS injection (Figure 4A, part a). In contrast, TUNEL-positive cells were rare in joints injected with rHuOPG (Figure 4A, part b). The number of TUNEL-positive chondrocytes in the joints of the OPG-treated group was almost one-third of that in the control group ($P < 0.05$) (Figure 4B). These data indicated that the anti-apoptotic effect of OPG functions to protect the articular cartilage.

Expression of OPG and TRAIL in chondrocytes of mice with experimentally induced OA. Immunohistochemical analysis indicated that while OPG could be detected in synovial cells and chondrocytes, OPG protein was observed at higher levels in the peripheral layers of OA joint cartilage and synovial tissue following OPG administration (Figure 5A). One of the OPG ligands, TRAIL, has also been observed in chondrocytes and synovial tissues from OA joints (18,19,22). Moreover, TRAIL is known to induce chondrocyte apoptosis in vitro (22,23). Our immunohistochemical analysis also

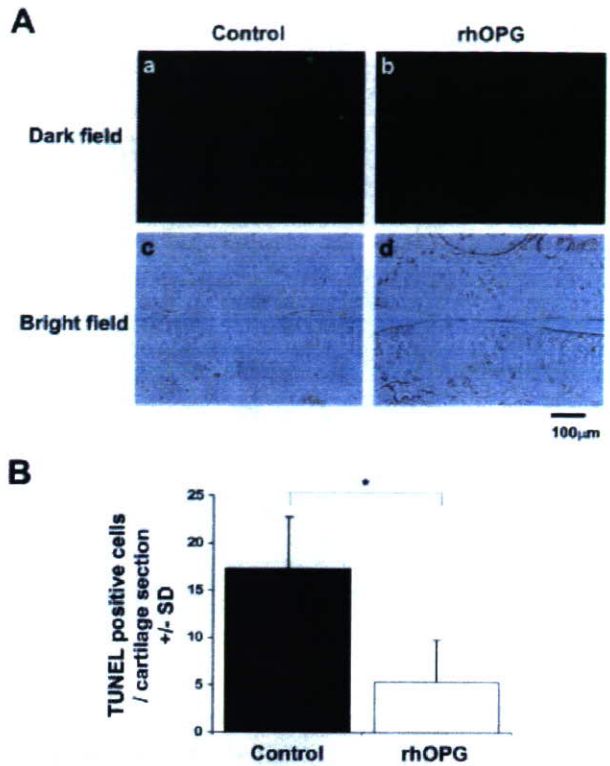

Figure 4. Analysis of apoptosis in TUNEL-stained sections of cartilage from mice with surgically induced osteoarthritis (OA) after intraarticular administration of recombinant human osteoprotegerin (rHuOPG) or vehicle. Intraarticular injection of rHuOPG (rhOPG) or vehicle alone (control) into mouse knee joints was performed 5 times a week beginning the day after surgery and continuing for 4 weeks thereafter. **A,** TUNEL staining of OA cartilage sections was examined by darkfield (**a** and **b**) and brightfield (**c** and **d**) microscopy. The number of TUNEL-positive cells was increased in knee joint cartilage from control mice (**a**) but was significantly reduced in knee joint cartilage from mice injected with rHuOPG (**b**). **B,** The number of TUNEL-positive cells per section of OA cartilage was determined under fluorescence microscopy. Values are the mean and SD of 5 mice per group. * = $P < 0.05$ by Mann-Whitney U test.

indicated that TRAIL was expressed in chondrocytes. TRAIL-positive chondrocytes were primarily detected in the periphery of the joint cartilage in OPG-treated animals (Figure 5B, part b), whereas they were present in the middle and deep zones of the joint cartilage, with hypertrophic differentiation, in control animals (Figure 5B, part a). The expression patterns of OPG and TRAIL overlapped significantly in the OPG-treated group (Figure 5A, part f, and Figure 5B, part b). These results suggest that exogenous OPG protected the articular chondrocytes by inhibiting TRAIL-induced apoptosis in vivo.

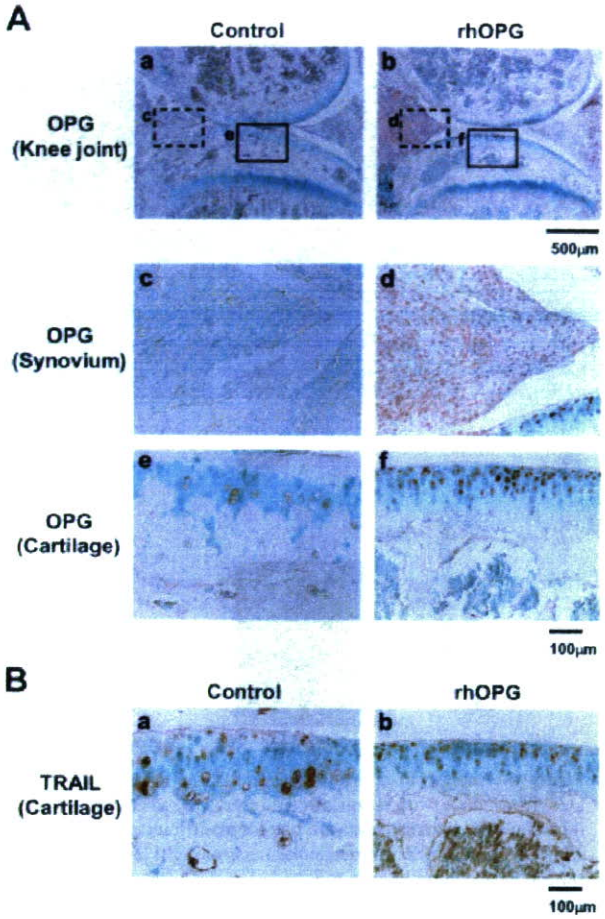

Figure 5. Expression of osteoprotegerin (OPG) and TRAIL in chondrocytes from mice with surgically induced osteoarthritis (OA) after intraarticular administration of recombinant human osteoprotegerin (rHuOPG) or vehicle. Intraarticular injection of rHuOPG (rhOPG) or vehicle alone (control) into mouse knee joints was performed 5 times a week beginning the day after surgery and continuing for 4 weeks thereafter. **A,** OPG protein was present at high levels in synovial cells (**d**) and cartilage chondrocytes (**f**) in sections from rHuOPG-treated mice, whereas only trace amounts of OPG protein were observed in control animals (**a**, **c**, and **e**). Control chondrocytes (**e**) showed hypertrophic changes as a result of OA progression, as compared with chondrocytes from rHuOPG-treated mice (**f**). Boxed and labeled areas in **a** and **b** are shown at higher magnification in **c** and **e** and in **d** and **f**, respectively. **B,** TRAIL expression was also observed in the cartilage chondrocytes of control (**a**) and OPG-treated (**b**) mice with surgically induced OA.

DISCUSSION

This study revealed the effects of reductions of endogenous OPG activity on the progression of instability-induced cartilage destruction in mice heterozygous for an OPG gene mutation. Previous studies have indicated that $OPG^{-/-}$ mice demonstrate severe destruction of growth plate cartilage and growth plate cartilage loss–induced epiphyseal and metaphyseal trabecular bone formation (14,15). Histologic examination revealed that at 8 weeks of age, $OPG^{-/-}$ mice exhibited irregular articular cartilage, including markedly thinned cartilage layers and invasion of the vasculature into the calcified layer (Figure 1C); in contrast, the articular cartilage of young adult $OPG^{+/-}$ mice was intact at this age (Figure 1B). Although $OPG^{+/-}$ mice exhibit a significant loss of total bone density compared with their WT littermates by the age of 6 months (mean ± SD 487.6 ± 27 mg/cm^3 versus 521.2 ± 29 mg/cm^3; $P < 0.05$), bone volume is comparable in young adult $OPG^{+/-}$ and WT mice at the ages evaluated in these experiments (13).

Since subchondral bone metabolism is important for the maintenance of articular cartilage (24), we chose young adult $OPG^{+/-}$ mice as our experimental OA model in which to examine the effects of OPG haploinsufficiency in chondrocytes on cartilage metabolism. After induction of OA in $OPG^{+/-}$ mice and their WT littermates, the $OPG^{+/-}$ mice exhibited severe articular cartilage degeneration as compared with the WT mice. This observation indicated that adequate OPG was required for the maintenance of cartilage and the prevention of mechanical stress–induced cartilage degeneration. The observation that the subchondral bone structures in $OPG^{+/-}$ mice and their WT littermates were histologically indistinguishable suggested that endogenous OPG likely plays only a minimal role in subchondral bone turnover in the acute phase of OA progression.

We also demonstrated that intraarticular administration of exogenous OPG effectively protected the articular cartilage from degradation. Although previous reports suggested a protective effect of OPG on cartilage in arthritis models, systemically administered OPG protected both the articular cartilage and articular bone (25–28). Therefore, it was unclear whether in arthritis, OPG affected chondrocyte metabolism directly or indirectly through osteoclastic bone erosion of subchondral bone via RANK signaling (27). To study this, we administered rHuOPG intraarticularly, which revealed the direct effect of this substance on articular chondrocyte metabolism.

TRAIL, one of the ligands for OPG, was also expressed in chondrocytes, as reported previously (22), regardless of OPG administration. OPG binds to TRAIL, a death domain–containing type II transmembrane protein member of the TNF superfamily (29,30). TRAIL constitutes a family of ligands that transduces death signals through a death domain–containing receptor (31). OPG inhibits TRAIL-induced apoptosis in

Jurkat cells (29) and endothelial cells (32). TRAIL also induces chondrocyte apoptosis in vitro; its expression is increased in the chondrocytes of rats with experimentally induced OA (22). In this study, OPG was observed in TRAIL-expressing chondrocytes and synovium in OPG-treated animals. These findings are consistent with the hypothesis that exogenously administered OPG prevents chondrocyte apoptosis in our model of surgically induced OA. Although inhibition of the TRAIL pathway by OPG may be one of the potent mechanisms of OA prevention of OPG, the target of OPG is still to be elucidated.

The concentration of OPG we used was determined according to previous observations in endothelial cells (32), where endothelial cell apoptosis induced by serum deprivation was blocked by OPG concentrations >0.5 μg/ml. The appropriate concentration of OPG will need to be determined for any future clinical applications.

TUNEL staining revealed that OPG administration significantly suppressed chondrocyte apoptosis. Exogenous OPG was confined to the cartilage and synovium; the subchondral bone volume and vascular invasion were not affected by intraarticular OPG administration. These observations indicated that the chondroprotective effect of OPG was independent of the subchondral bone protection.

To investigate the function of OPG in articular chondrocyte metabolism, we used an experimental stress-induced murine model of OA that is reproducible and closely resembles OA in humans (1). The combination of medial collateral ligament transection and medial meniscectomy induced medial tibial cartilage destruction within 4 weeks. The early changes in the articular cartilage after surgery resulted from a defect in the superficial zone and corresponded to a decrease in Safranin O staining. These initial findings were followed by progressive cartilage destruction in a manner identical to that reported for OA pathology in humans as determined by arthroscopic and histologic analyses (33,34). Along with the catabolic changes, the anabolic reactions of chondrocyte proliferation and subchondral sclerosis were also observed in our model.

The findings of this study cannot rule out the importance of subchondral bone metabolism in articular cartilage protection. Although articular chondrocytes do not have an intact RANK signaling apparatus, RANKL-deficient mice have been shown to be protected from bone erosion in a serum-transfer model of arthritis (35), indicating that OPG protects articular cartilage via maintenance of subchondral bone. In the rat inflammatory arthritis model, systemic administration of OPG preserved articular cartilage (25,27). While significant chondroprotection was observed in mildly inflamed joints following administration of Fc-OPG, no significant protection was seen in the more severely inflamed joints of rats treated with OPG. Similarly, in a serum-transfer model of arthritis, RANKL-deficient mice exhibited cartilage loss despite protection from bone erosion and despite partial inhibition of cartilage destruction (35). In these experiments, OPG was administered systemically; intraarticular OPG levels were not affected (27). Administration of OPG both systemically and intraarticularly may have an additive effect on chondrocyte protection in arthritis.

Bone resorption inhibitors, including bisphosphonates and calcitonin, have been shown to reduce cartilage degradation in experimental arthritis models (36,37). In a rat model of stress-induced OA, alendronate was shown to have a partial chondroprotective effect during the early stages of disease (36). Although the direct target of bisphosphonates is not known, bisphosphonate inhibition of subchondral bone turnover may be a candidate mechanism that would explain this phenomenon. Bisphosphonates may indirectly reduce cartilage breakdown by altering the distribution of mechanical stress. Bisphosphonate inhibition of osteoclastic bone resorption may also reduce the release of inflammatory cytokines and growth factors (36).

In conclusion, we have demonstrated that rHuOPG prevents cartilage destruction in an experimental murine model of OA and that endogenous OPG protects against cartilage destruction during the progression of OA. Our results provide clues that OPG prevents chondrocyte apoptosis via a direct effect on chondrocytes in vivo. These results support a potential therapeutic application of rHuOPG in human OA.

ACKNOWLEDGMENTS

The authors would like to acknowledge Dr. Satoru Kamekura for technical advice with the experimental OA model and Miyoko Ojima for expert help with the histologic analyses.

AUTHOR CONTRIBUTIONS

Dr. Asou had full access to all of the data in the study and takes responsibility for the integrity of the data and the accuracy of the data analysis.

Study design. Asou, Chung, Kawaguchi.

Acquisition of data. Shimizu, Itoh.

Analysis and interpretation of data. Asou, Chung, Kawaguchi, Muneta.

Manuscript preparation. Shimizu, Asou, Shinomiya.

Statistical analysis. Shimizu.

REFERENCES

1. Kamekura S, Hoshi K, Shimaoka T, Chung U, Chikuda H, Yamada T, et al. Osteoarthritis development in novel experimental mouse models induced by knee joint instability. Osteoarthritis Cartilage 2005;13:632–41.
2. Hashimoto S, Ochs RL, Komiya S, Lotz M. Linkage of chondrocyte apoptosis and cartilage degradation in human osteoarthritis. Arthritis Rheum 1998;41:1632–8.
3. Kim HA, Lee YJ, Seong SC, Choe KW, Song YW. Apoptotic chondrocyte death in human osteoarthritis. J Rheumatol 2000;27: 455–62.
4. Amin AR, Abramson SB. The role of nitric oxide in articular cartilage breakdown in osteoarthritis. Curr Opin Rheumatol 1998; 10:263–8.
5. Hashimoto S, Takahashi K, Amiel D, Coutts RD, Lotz M. Chondrocyte apoptosis and nitric oxide production during experimentally induced osteoarthritis. Arthritis Rheum 1998;41:1266–74.
6. Tsuda E, Goto M, Mochizuki S, Yano K, Kobayashi F, Morinaga T, et al. Isolation of a novel cytokine from human fibroblasts that specifically inhibits osteoclastogenesis. Biochem Biophys Res Commun 1997;234:137–42.
7. Yasuda H, Shima N, Nakagawa N, Yamaguchi K, Kinosaki M, Mochizuki S, et al. Osteoclast differentiation factor is a ligand for osteoprotegerin/osteoclastogenesis-inhibitory factor and is identical to TRANCE/RANKL. Proc Natl Acad Sci U S A 1998;95: 3597–602.
8. Yasuda H, Shima N, Nakagawa N, Mochizuki SI, Yano K, Fujise N, et al. Identity of osteoclastogenesis inhibitory factor (OCIF) and osteoprotegerin (OPG): a mechanism by which OPG/OCIF inhibits osteoclastogenesis in vitro. Endocrinology 1998;139: 1329–37.
9. Lacey DL, Tan HL, Lu J, Kaufman S, Van G, Qiu W, et al. Osteoprotegerin ligand modulates murine osteoclast survival in vitro and in vivo. Am J Pathol 2000;157:435–48.
10. Burr DB. Anatomy and physiology of the mineralized tissues: role in the pathogenesis of osteoarthrosis. Osteoarthritis Cartilage 2004;12 Suppl A: S20–30.
11. Yano K, Tsuda E, Washida N, Kobayashi F, Goto M, Harada A, et al. Immunological characterization of circulating osteoprotegerin/osteoclastogenesis inhibitory factor: increased serum concentrations in postmenopausal women with osteoporosis. J Bone Miner Res 1999;14:518–27.
12. Mizuno A, Amizuka N, Irie K, Murakami A, Fujise N, Kanno T, et al. Severe osteoporosis in mice lacking osteoclastogenesis inhibitory factor/osteoprotegerin. Biochem Biophys Res Commun 1998;247:610–5.
13. Bucay N, Sarosi I, Dunstan CR, Morony S, Tarpley J, Capparelli C, et al. Osteoprotegerin-deficient mice develop early onset osteoporosis and arterial calcification. Genes Dev 1998;12:1260–8.
14. Amizuka N, Shimomura J, Li M, Seki Y, Oda K, Henderson JE, et al. Defective bone remodelling in osteoprotegerin-deficient mice. J Electron Microsc (Tokyo) 2003;52:503–13.
15. Kawana F, Sasaki T. Osteoclast differentiation and characteristic trabecular bone formation during growth plate destruction in osteoprotegerin-deficient mice. J Electron Microsc (Tokyo) 2003; 52:515–25.
16. Daroszewska A, Ralston SH. Genetics of Paget's disease of bone. Clin Sci (Lond) 2005;109:257–63.
17. Van Staa TP, Selby P, Leufkens HG, Lyles K, Sprafka JM, Cooper C. Incidence and natural history of Paget's disease of bone in England and Wales. J Bone Miner Res 2002;17:465–71.
18. Komuro H, Olee T, Kuhn K, Quach J, Brinson DC, Shikhman A, et al. The osteoprotegerin/receptor activator of nuclear factor κB/receptor activator of nuclear factor κB ligand system in cartilage. Arthritis Rheum 2001;44:2768–76.
19. Haynes DR, Barg E, Crotti TN, Holding C, Weedon H, Atkins GJ, et al. Osteoprotegerin expression in synovial tissue from patients with rheumatoid arthritis, spondyloarthropathies and osteoarthritis and normal controls. Rheumatology (Oxford) 2003;42:123–34.
20. Mankin HJ, Dorfman H, Lippiello L, Zarins A. Biochemical and metabolic abnormalities in articular cartilage from osteo-arthritic human hips. II. Correlation of morphology with biochemical and metabolic data. J Bone Joint Surg Am 1971;53:523–37.
21. Mankin HJ. Biochemical and metabolic abnormalities in osteoarthritic human cartilage. Fed Proc 1973;32:1478–80.
22. Lee SW, Lee HJ, Chung WT, Choi SM, Rhyu SH, Kim DK, et al. TRAIL induces apoptosis of chondrocytes and influences the pathogenesis of experimentally induced rat osteoarthritis. Arthritis Rheum 2004;50:534–42.
23. Pettersen I, Figenschau Y, Olsen E, Bakkelund W, Smedsrod B, Sveinbjornsson B. Tumor necrosis factor-related apoptosis-inducing ligand induces apoptosis in human articular chondrocytes in vitro. Biochem Biophys Res Commun 2002;296:671–6.
24. Hayami T, Pickarski M, Zhuo Y, Wesolowski GA, Rodan GA, Duong LT. Characterization of articular cartilage and subchondral bone changes in the rat anterior cruciate ligament transection and meniscectomized models of osteoarthritis. Bone 2006;38:234–43.
25. Kong YY, Feige U, Sarosi I, Bolon B, Tafuri A, Morony S, et al. Activated T cells regulate bone loss and joint destruction in adjuvant arthritis through osteoprotegerin ligand. Nature 1999; 402:304–9.
26. Redlich K, Hayer S, Maier A, Dunstan CR, Tohidast-Akrad M, Lang S, et al. Tumor necrosis factor α-mediated joint destruction is inhibited by targeting osteoclasts with osteoprotegerin. Arthritis Rheum 2002;46:785–92.
27. Romas E, Sims NA, Hards DK, Lindsay M, Quinn JW, Ryan PF, et al. Osteoprotegerin reduces osteoclast numbers and prevents bone erosion in collagen-induced arthritis. Am J Pathol 2002;161: 1419–27.
28. Campagnuolo G, Bolon B, Feige U. Kinetics of bone protection by recombinant osteoprotegerin therapy in Lewis rats with adjuvant arthritis. Arthritis Rheum 2002;46:1926–36.
29. Emery JG, McDonnell P, Burke MB, Deen KC, Lyn S, Silverman C, et al. Osteoprotegerin is a receptor for the cytotoxic ligand TRAIL. J Biol Chem 1998;273:14363–7.
30. Wiley SR, Schooley K, Smolak PJ, Din WS, Huang CP, Nicholl JK, et al. Identification and characterization of a new member of the TNF family that induces apoptosis. Immunity 1995;3:673–82.
31. Schulze-Osthoff K, Ferrari D, Los M, Wesselborg S, Peter ME. Apoptosis signaling by death receptors. Eur J Biochem 1998;254: 439–59.
32. Pritzker LB, Scatena M, Giachelli CM. The role of osteoprotegerin and tumor necrosis factor-related apoptosis-inducing ligand in human microvascular endothelial cell survival. Mol Biol Cell 2004;15:2834–41.
33. Poole AR. An introduction to the pathophysiology of osteoarthritis. Front Biosci 1999;4:D662–70.
34. Santori N, Villar RN. Arthroscopic findings in the initial stages of hip osteoarthritis. Orthopedics 1999;22:405–9.
35. Pettit AR, Ji H, von Stechow D, Muller R, Goldring SR, Choi Y, et al. TRANCE/RANKL knockout mice are protected from bone erosion in a serum transfer model of arthritis. Am J Pathol 2001;159:1689–99.
36. Hayami T, Pickarski M, Wesolowski GA, Mclane J, Bone A, Destefano J, et al. The role of subchondral bone remodeling in osteoarthritis: reduction of cartilage degeneration and prevention of osteophyte formation by alendronate in the rat anterior cruciate ligament transection model. Arthritis Rheum 2004;50:1193–206.
37. Myers SL, Brandt KD, Burr DB, O'Connor BL, Albrecht M. Effects of a bisphosphonate on bone histomorphometry and dynamics in the canine cruciate deficiency model of osteoarthritis. J Rheumatol 1999;26:2645–53.

OPEN ACCESS Freely available online

PLoS one

Akt1 in Osteoblasts and Osteoclasts Controls Bone Remodeling

Naohiro Kawamura[1], Fumitaka Kugimiya[1], Yasushi Oshima[1], Shinsuke Ohba[2], Toshiyuki Ikeda[1], Taku Saito[1], Yusuke Shinoda[1], Yosuke Kawasaki[1], Naoshi Ogata[1], Kazuto Hoshi[1], Toru Akiyama[1], William S. Chen[3], Nissim Hay[4], Kazuyuki Tobe[5], Takashi Kadowaki[5], Yoshiaki Azuma[6], Sakae Tanaka[1], Kozo Nakamura[1], Ung-il Chung[2], Hiroshi Kawaguchi[1]*

1 Department of Sensory and Motor System Medicine, Faculty of Medicine, University of Tokyo, Tokyo, Japan, 2 Center for Disease Biology and Integrative Medicine, Faculty of Medicine, University of Tokyo, Tokyo, Japan, 3 Transgenic and Knockout Mouse Laboratory, University of Kansas, Lawrence, Lawrence, Kansas, United States of America, 4 Department of Molecular Genetics, College of Medicine, University of Illinois at Chicago, Chicago, Illinois, United States of America, 5 Department of Metabolic Diseases, Faculty of Medicine, University of Tokyo, Tokyo, Japan, 6 Teijin Institute for Biomedical Research, Tokyo, Japan

Bone mass and turnover are maintained by the coordinated balance between bone formation by osteoblasts and bone resorption by osteoclasts, under regulation of many systemic and local factors. Phosphoinositide-dependent serine-threonine protein kinase Akt is one of the key players in the signaling of potent bone anabolic factors. This study initially showed that the disruption of Akt1, a major Akt in osteoblasts and osteoclasts, in mice led to low-turnover osteopenia through dysfunctions of both cells. Ex vivo cell culture analyses revealed that the osteoblast dysfunction was traced to the increased susceptibility to the mitochondria-dependent apoptosis and the decreased transcriptional activity of runt-related transcription factor 2 (Runx2), a master regulator of osteoblast differentiation. Notably, our findings revealed a novel role of Akt1/forkhead box class O (FoxO) 3a/Bim axis in the apoptosis of osteoblasts: Akt1 phosphorylates the transcription factor FoxO3a to prevent its nuclear localization, leading to impaired transactivation of its target gene Bim which was also shown to be a potent proapoptotic molecule in osteoblasts. The osteoclast dysfunction was attributed to the cell autonomous defects of differentiation and survival in osteoclasts and the decreased expression of receptor activator of nuclear factor-κB ligand (RANKL), a major determinant of osteoclastogenesis, in osteoblasts. Akt1 was established as a crucial regulator of osteoblasts and osteoclasts by promoting their differentiation and survival to maintain bone mass and turnover. The molecular network found in this study will provide a basis for rational therapeutic targets for bone disorders.

Citation: Kawamura N, Kugimiya F, Oshima Y, Ohba S, Ikeda T, et al (2007) Akt1 in Osteoblasts and Osteoclasts Controls Bone Remodeling. PLoS ONE 2(10): e1058. doi:10.1371/journal.pone.0001058

INTRODUCTION

Bone is continually remodeled according to physiological circumstances through bone formation by osteoblasts and bone resorption by osteoclasts, and bone mass and turnover are maintained by their coordinated balance in healthy adults. Many systemic and local factors are involved in the regulation [1,2], among which insulin, insulin-like growth factor-I (IGF-I), bone morphogenetic factors (BMPs), and Wnt proteins are potent bone anabolic factors [3–6]. A serine-threonine kinase Akt, also called protein kinase B (PKB), is known as a potent signal transducer of these bone anabolic factors [7–9].

There are three Akt family members, Akt1/PKBα, Akt2/PKBβ and Akt3/PKBγ. Akt1 and Akt2, but not Akt3, are reported to be ubiquitously and similarly expressed in various tissues, although Akt2 is expressed more predominantly in insulin target tissues such as fat, liver and muscle [9,10]. Accordingly, Akt1-/- mice and Akt2-/- mice show similar phenotypes including dwarfism, except that only the latter exhibit severe diabetes [10–13]. Although phenotype of mice lacking single Akt isoform is relatively mild possibly due to functional redundancy of the remaining isoforms, double-knockout of Akt1 and Akt2 in mice causes severely impaired bone development and death shortly after birth [14]. The abnormalities of these knockout mice certainly imply a crucial commitment of Akt signals to bone metabolism, yet it has remained unknown whether or not these were due to the cell autonomous effects of the Akt deficiency on bone cells. To elucidate the physiological role of the Akt signaling in the regulation of bone formation and resorption, the present study initially analyzed the bones of mice lacking Akt1, a major Akt isoform in bone, and found that the deficiency caused osteopenia with a low turnover state. We further investigated the underlying cellular and molecular mechanisms in osteoblasts and osteoclasts.

RESULTS

Akt1 is a major isoform in bone cells

We initially confirmed that the total Akt (Akt1–3) was phosphorylated by osteogenic factors IGF-I and BMP-2 in cultured osteoblasts, and by a bone resorptive macrophage colony-stimulating factor (M-CSF) in osteoclast-progenitor bone marrow macrophages (BMM) and mature osteoclasts (Supp. Fig S1A). Among the three Akt isoforms, Akt1 and Akt2 were highly expressed in these bone cells (Supp. Fig S1B).

Academic Editor: Thomas Zwaka, Baylor College of Medicine, United States of America

Received May 8, 2007; **Accepted** August 14, 2007; **Published** October 24, 2007

Funding: This study was supported by a Grant-in-aid for Scientific Research from the Japanese Ministry of Education, Culture, Sports, Science, and Technology (#17390410). The sponsor had no role in study design, data collection, data analysis, data interpretation, or writing of the report.

Competing Interests: The authors have declared that no competing interests exist.

* **To whom correspondence should be addressed.** E-mail: kawaguchi-ort@h.u-tokyo.ac.jp

Akt1 deficiency causes decreased bone mass and formation

To investigate the physiological role of the Akt signaling in bone, we examined the bone phenotype of Akt1 deficient (Akt1-/-) mice, because Akt1; Akt2 double-knockout mice die shortly after birth [14]. Akt1-/- mice were healthy and fertile without abnormality in major organs or skeletal patterning, but were smaller in size compared to the wild-type (WT) littermates (Supp. Fig S2) as previously reported [11]. Radiological analyses of long bones in 8 week-old mice using plain X-ray, bone mineral density (BMD) analysis (Fig 1A), three dimensional (3D) CT (Fig 1B), and peripheral quantitative CT (pQCT) (Fig 1C) revealed decreases in both trabecular and cortical bones as a result of the Akt1 deficiency. Although the growth plate was not affected (Fig 1D), bone formation parameters (MAR&BFR) of the trabecular bone were decreased (Fig 1E), indicating that osteopenia in the Akt1-/- mice was at least partly due to the impairment of osteoblastic bone formation. This defect was accompanied by a decrease in the number of osteoblasts shown by the percentage of bone surface covered by cuboidal osteoblasts (Ob.S/BS) and an increase in that of apoptotic osteoblasts shown by terminal deoxynucleotidyl transferase mediated dUTP nick-end-labeling (TUNEL)-positive cells (Fig 1E).

Akt1 deficiency enhances susceptibility to apoptosis of osteoblasts via FoxO3a

To learn the mechanism of impaired bone formation, we compared ex vivo functions of osteoblasts isolated from WT and Akt1-/- littermates. We first confirmed that both phosphorylated and unphosphorylated Akt proteins were considerably decreased in cultured Akt1-/- osteoblasts without compensatory increase of Akt2 protein, indicating a substantial suppression of the total Akt signaling by depletion of an isoform Akt1 in osteoblasts (Fig 2A). Although cell proliferation was not affected (Fig 2B), cell survival after serum deprivation was decreased by the Akt1 deficiency (Fig 2C). This decrease was confirmed to be due to the enhanced susceptibility to apoptosis of osteoblasts by TUNEL staining (Fig 2D). Caspase-3 activity and the cleaved active form was enhanced in Akt1-/- osteoblasts, which was restored by adenoviral introduction of a constitutively active form of Akt1 ($Akt1^{CA}$) or Bcl-x_L, a specific inhibitor of mitochondria-dependent apoptosis [15] (Fig 2E). Hence, Akt1 deficiency in osteoblasts is not likely to affect the proliferation, but suppresses the survival through an enhanced susceptibility to mitochondria-dependent apoptosis.

Among apoptosis-related molecules that have been reported to be possible substrates of Akt [9,16], transcription factors FoxO3a and FoxO1, and a proapoptotic molecule Bad were expressed in primary osteoblasts and osteoblastic cell line MC3T3-E1 (Fig 2F). Since phosphorylation of FoxO proteins is known to result in their nuclear exclusion in other types of cells [16], we confirmed the nuclear entry of FoxO3a after serum deprivation in MC3T3-E1 cells (Supp. Fig S3). The nuclear localization of FoxO3a was more enhanced in Akt1-/- osteoblasts than in WT after serum deprivation (Fig 2G). This correlated with the decrease of the upper band and the increase of the lower band in the cytoplasmic fraction of the immunoblotting, which were proved to be phosphorylated and unphosphorylated FoxO3a, respectively, since the upper one was enhanced by FBS and eliminated by lambda protein phosphatase (Fig 2H). Meanwhile, Akt1 overexpression by $Akt1^{CA}$ transfection in osteoblasts stimulated the cytoplasmic FoxO3a phosphorylation and inhibited the nuclear entry (Fig 2I). Contrarily, subcellular localization of FoxO1 was not affected by the Akt1 deficiency (Fig 2G), nor was phosphorylated Bad protein detected in osteoblasts, probably due to its low level (data not shown). Finally, the decreased survival rate and the increased caspase-3 activity of Akt1-/- osteoblasts after serum deprivation were restored by introduction of a dominant-negative form of FoxO3a ($FoxO3a^{DN}$) (Fig 2J, K).

The lines of results indicate that a transcription factor FixO3a is a phosphorylation target of Akt1 in the anti-apoptotic action on osteoblasts, so that the Akt1 deficiency attenuates FoxO3a phosphorylation and nuclear exclusion, which leads to the enhanced transcriptional activity somehow causing apoptosis.

Akt1 suppresses osteoblast apoptosis through inhibition of FoxO3a and Bim

We next sought to identify the transcriptional target of FoxO3a that lies downstream of the Akt1 anti-apoptotic signaling in osteoblasts. Among the candidate molecules Fas ligand, Bim, and Bcl-x_L that were reported previously in other tissues [17], only Bim mRNA level was increased after serum deprivation in osteoblasts (Fig 3A). Bim protein level was also increased, followed by the induction of cleaved caspase-3, while none of the major regulators of mitochondria-dependent apoptosis: proapoptotic Bax, anti-apoptotic Bcl-2 and Bcl-x_L [15], was affected by serum deprivation (Fig 3B). The cleaved caspase-3 induction was mediated by Bim, since it was suppressed by silencing of Bim through RNA interference (Fig 3C). Actinomycin D, an inhibitor of RNA transcripion, canceled the Bim increase after serum deprivation, indicating that this is a transcriptional induction (Supp. Fig S4A, B). The Bim promoter activity was actually enhanced by FoxOs, among which FoxO3a exhibited the strongest transactivity (Fig 3D). Endogenous Bim expression was confirmed to be enhanced by FoxO3a overexpression and attenuated by the suppression (Fig 3E, F). These results indicate that Bim is a transcriptional target of FoxO3a in osteoblasts.

We then looked at the involvement of Akt1 in the FoxO3a and Bim interaction in osteoblasts. Gain-of-function of Akt1 by $Akt1^{CA}$ transfection abrogated the stimulation of the Bim promoter activity by FoxO3a (Fig 3G). The induction of endogenous Bim after serum deprivation was also suppressed by $Akt1^{CA}$ (Fig 3H) as well as by insulin or IGF-I, potent activators of the Akt signaling (Supp. Fig S4C). Finally, the Bim expression in Akt1-/- osteoblasts was higher than that in WT osteoblasts, which was restored by the $FoxO3a^{DN}$ transfection (Fig 3I).

Taken together, we conclude that Akt1 phosphorylates FoxO3a to prevent it from translocating into nucleus, which leads to suppression of Bim transactivation and osteoblast apoptosis.

Akt1 deficiency impairs Runx2-dependent differentiation and function of osteoblasts

Since the in vivo histomorphometric analysis of the Alt1-/- bone (Fig 1E) showed not only a decrease in osteoblast number, but also a decrease in the ability of an individual osteoblast to form bone (MAR), we performed ex vivo analyses of the effects of Akt1 deficiency on osteoblast differentiation and function, in addition to their proliferation and apoptosis. The differentiation determined by alkaline phosphatase (ALP) activity was impaired in Akt1-/- osteoblasts in the control and stimulated cultures by insulin or IGF-I, but not by BMP-2 (Fig 4A). Differentiation markers type I collagen, ALP, bone sialoprotein, osteocalcin, Runx2 and osterix were also decreased by Akt1 deficiency in osteoblasts (Fig 4B). This was a cell autonomous function of Akt1 since the impaired differentiation and matrix synthesis shown by ALP and Alizarin red stainings in the Akt1-/- osteoblast culture were restored by introduction of $Akt1^{CA}$ (Fig 4C). Interestingly, the $Akt1^{CA}$

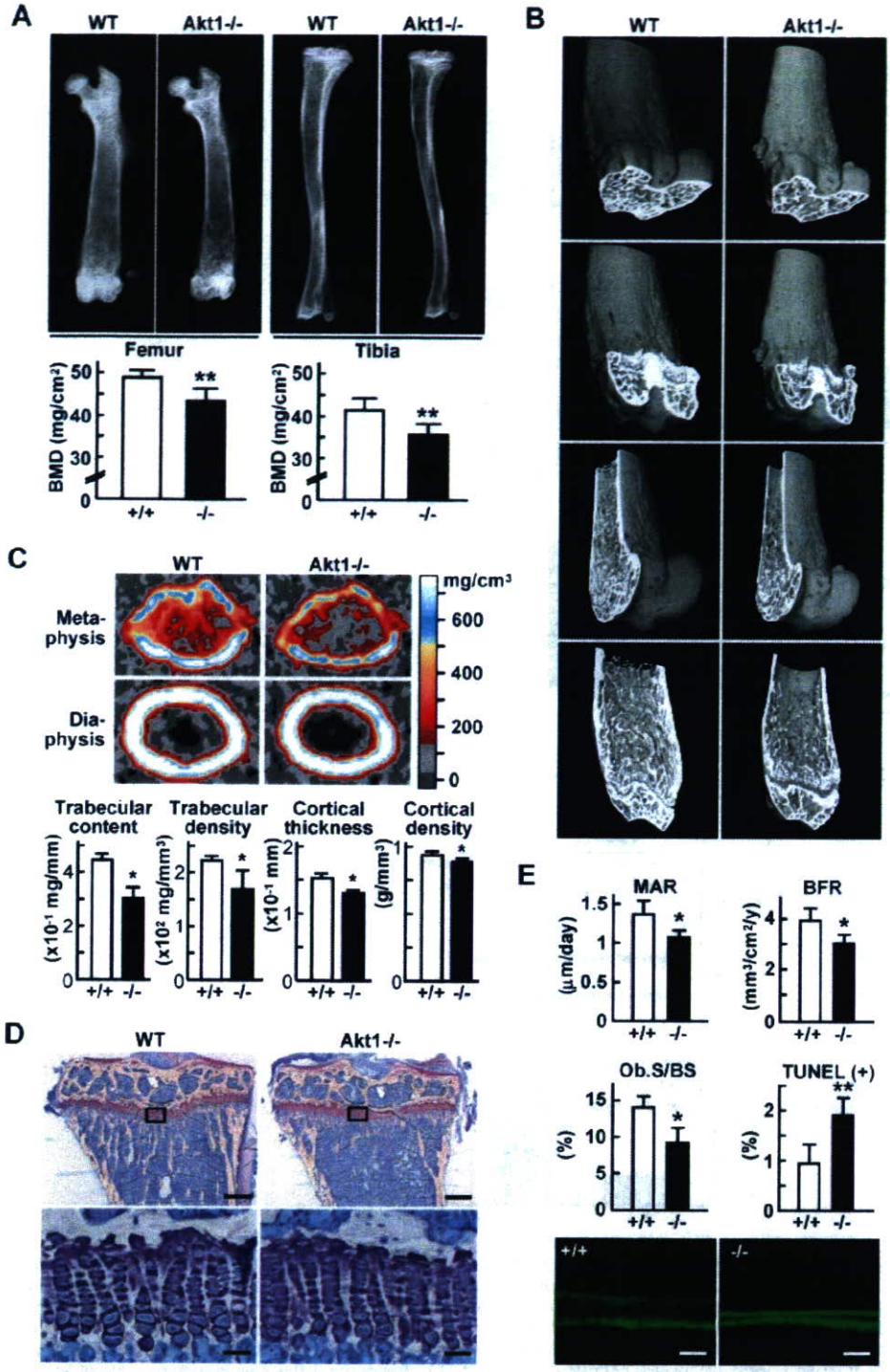

Figure 1. Bone mass and formation are decreased in Akt1-/- mice. (A) Plain X-ray images of femur and tibia in WT and Akt1-/- male littermates at 8 weeks of age. The BMD of the entire femurs and tibias measured by DXA is shown in the graphs below. Data are expressed as means (bars)±SEM (error bars) for 5 WT and 3 Akt1-/- littermates. **P<0.01 vs. WT. (B) Three-dimensional CT images of distal femurs. (C) pQCT images of the distal metaphysis and the mid-diaphysis of the femurs. The color gradient indicating BMD is shown in the right bar. The trabecular content and density at the metaphysis, and the cortical thickness and density at the diaphysis are shown in the graphs below. Data are expressed as means (bars)±SEM (error bars) for 4 mice/group. *P<0.05 vs. WT. (D) Toluidine blue staining of the proximal tibias. Inset boxes indicate the regions of the bottom figures. The growth plate heights were 94.7±2.9 and 95.8±3.8 μm for WT and Akt1-/-, respectively (mean±SEM of 4 mice/group). Bars, 200 μm (top)&30 μm (bottom). (E) Bone formation parameters in histomorphometric analysis at the proximal tibias. MAR, mineral apposition rate; BFR/BS, bone formation rate per bone surface; Ob.S/BS, osteoblast surface per bone surface; TUNEL(+), percentage of TUNEL-positive apoptotic osteoblasts. Data are expressed as means (bars)±SEM (error bars) for 3–4 mice/group. *P<0.05, **P<0.01 vs. WT. The bottom figures show the representative calcein double labelings; bars, 20 μm.

doi:10.1371/journal.pone.0001058.g001

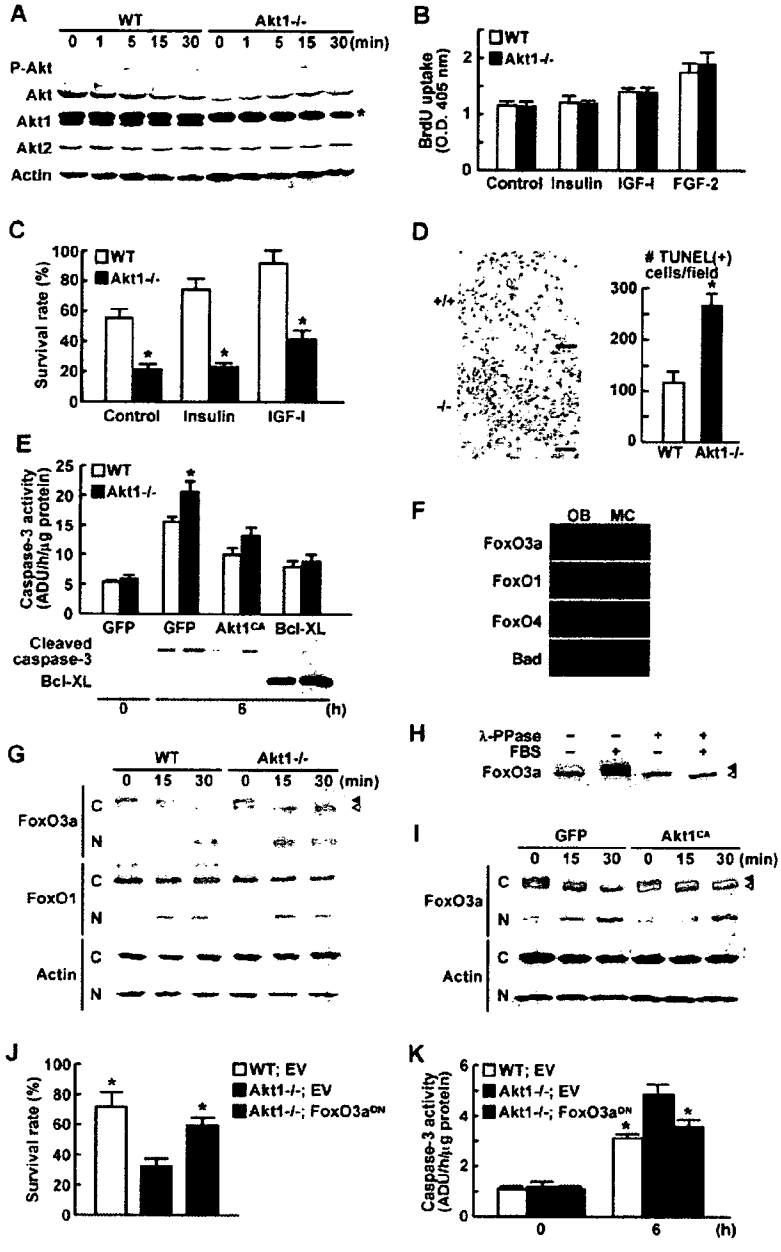

Figure 2. Akt1-/- osteoblasts are susceptibile to apoptosis via FoxO3a. (A) Time course of phosphorylated total Akt (P-Akt), total Akt (Akt), Akt1, Akt2, and β-actin levels after IGF-I stimulation determined by Western blotting in cultured calvarial osteoblasts from WT and Akt1-/- mice. An asterisk indicates a nonspecific band detected by an antibody to Akt1. (B) Cell proliferation determined by BrdU uptake into calvarial osteoblasts of two genotypes cultured with and without insulin, IGF-I, or FGF-2. Data are expressed as means (bars)±SEM (error bars) for 6 wells/group. (C) Survival rate of WT and Akt1-/- osteoblasts 48 h after serum deprivation in cultures with and without insulin or IGF-I. Data are expressed as means (bars)±SEM (error bars) for 6 wells/group. *P<0.01 vs. WT. (D) The number of TUNEL-positive osteoblasts per field (6×10^5 μm^2) 24 h after serum deprivation in cultured calvarial osteoblasts. Data are expressed as means (bars)±SEM (error bars) of 3 wells/group. *P<0.01 vs. WT. Bars, 100 μm. (E) Caspase-3 activity (top graph) and Western blotting for cleaved caspase-3 and Bcl-x_L (bottom) in WT and Akt1-/- osteoblasts adenovirally transfected with GFP, Akt1^{CA}, and Bcl-x_L before and 6 h after serum deprivation. Data are expressed as means (bars)±SEM (error bars) for 3 wells/group. *P<0.05 vs. WT. ADU: arbitrary densitometry unit. (F) FoxO3a, FoxO1, FoxO4 and Bad expressions determined by RT-PCR in primary mouse calvarial osteoblasts (OB) and MC3T3-E1 cells (MC). (G) Time course of FoxO3a, FoxO1, and β-actin levels by Western blotting after serum deprivation in the cytoplasmic (C) and nuclear (N) fractions of cultured WT and Akt1-/- osteoblasts. Closed and open arrowheads indicate phosphorylated and unphosphorylated FoxO3a, respectively. (H) Western blotting for FoxO3a in the cytoplasmic fraction of WT osteoblasts cultured with and without 10% FBS for 30 min. The lysates were treated with and without lambda protein phosphatase (λ-PPase). (I) Time course of FoxO3a and β-actin levels by Western blotting after serum deprivation in the cytoplasmic (C) and nuclear (N) fractions of cultured osteoblasts adenovirally transfected with GPF or Akt1^{CA}. (J) Survival rate of WT and Akt1-/- osteoblasts retrovirally transfected with empty vector (EV) or FoxO3a^{DN} 48 h after serum deprivation. Data are expressed as means (bars)±SEM (error bars) for 6 wells/group. *P<0.05 vs. Akt1-/- with EV. (K) Caspase-3 activity of WT and Akt1-/- osteoblasts retrovirally transfected with EV or FoxO3a^{DN} before and 6 h after serum deprivation. Data are expressed as means (bars)±SEM (error bars) for 3 wells/group. *P<0.05 vs. Akt1-/- with EV. ADU: arbitrary densitometry unit.
doi:10.1371/journal.pone.0001058.g002

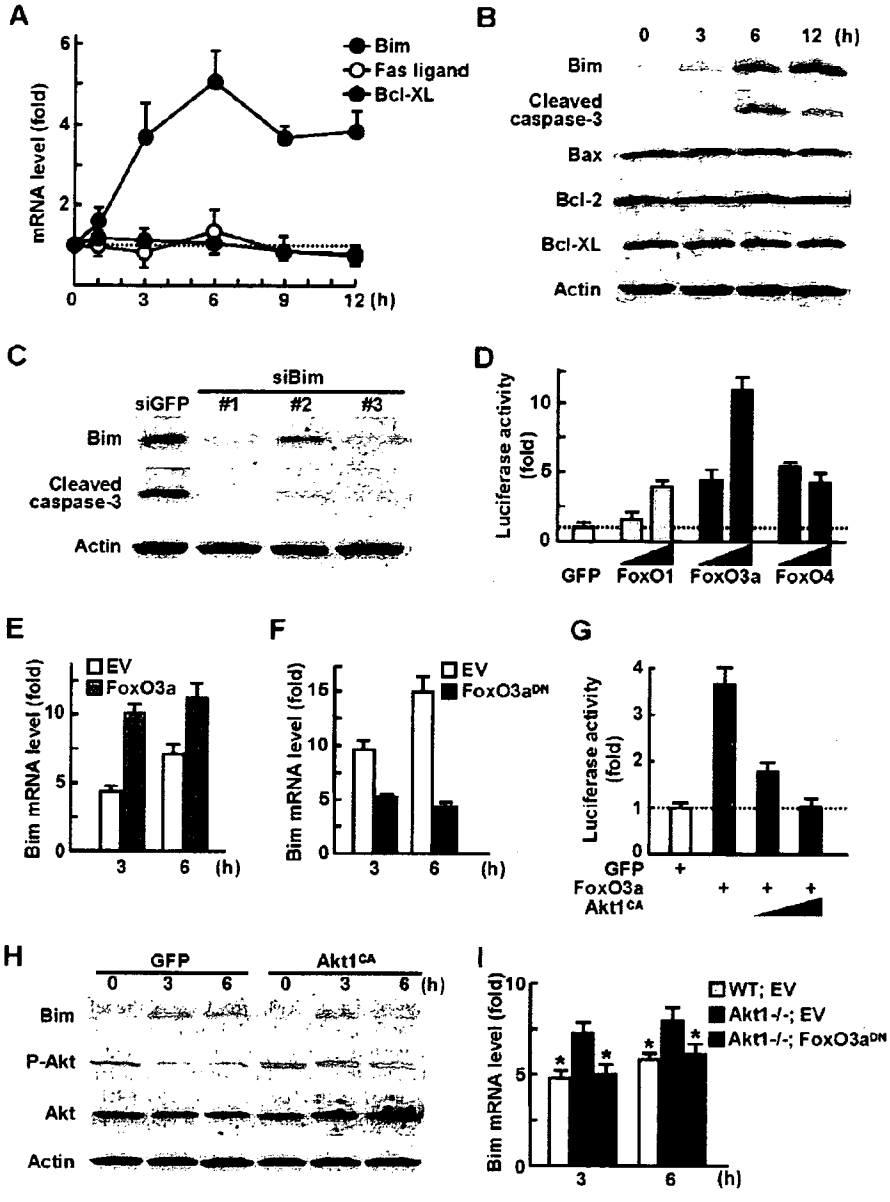

Figure 3. Akt1 suppresses osteoblast apoptosis via inhibition of FoxO3a and Bim. (A) Time course of mRNA levels determined by real-time RT-PCR of Bim, Fas ligand, and Bcl-x_L after serum deprivation in cultured calvarial osteoblasts. Data are normalized to those of β-actin and are expressed as means (symbols)±SEM (error bars) of the relative amount compared to time 0. (B) Time course of Bim, cleaved caspase-3, Bax, Bcl-2, Bcl-x_L, and β-actin levels determined by Western blotting after serum deprivation in cultured calvarial osteoblasts. (C) Western blotting for Bim, cleaved caspase-3, and β-actin levels 6 h after serum deprivation in MC3T3-E1 cells retrovirally transfected with three kinds of Bim siRNA or the control GFP siRNA. (D) Bim promoter activity determined by luciferase reporter assay in cultured MC3T3-E1 cells transfected with luciferase reporter constructs containing a 2-Kb Bim 5′-end flanking region. Plasmid vectors of the control GFP, FoxO1, FoxO3a, and FoxO4 were co-transfected in increasing amounts. Data are expressed as means (bars)±SEM (error bars) of the fold change compared to GFP. (E, F) Bim mRNA level determined by real-time RT-PCR 3 h and 6 h after serum deprivation in MC3T3-E1 cells retrovirally transfected with FoxO3a (E), FoxO3a^{DN} (F), or the respective EV. Data are normalized to those of β-actin and are expressed as means (bars)±SEM (error bars) of the relative amount compared to time 0. (G) Bim promoter activity analysis in MC3T3-E1 cells transfected with the control GFP, FoxO3a, and Akt1^{CA} plasmid vectors in increasing amounts. Data are expressed as means (bars)±SEM (error bars) of the fold change compared to GFP. (H) Time course of Bim, phosphorylated total Akt (P-Akt), total Akt (Akt), and β-actin levels determined by Western blotting after serum deprivation in cultured calvarial osteoblasts adenovirally transfected with GPF or Akt1^{CA}. (I) Bim mRNA level determined by real-time RT-PCR 3 h and 6 h after serum deprivation in cultured WT and Akt1-/- osteoblasts retrovirally transfected with EV or FoxO3a^{DN}. Data are normalized to those of β-actin and are expressed as means (bars)±SEM (error bars) of the relative amount compared to time 0. *P<0.05 vs. Akt1-/- with EV.

doi:10.1371/journal.pone.0001058.g003

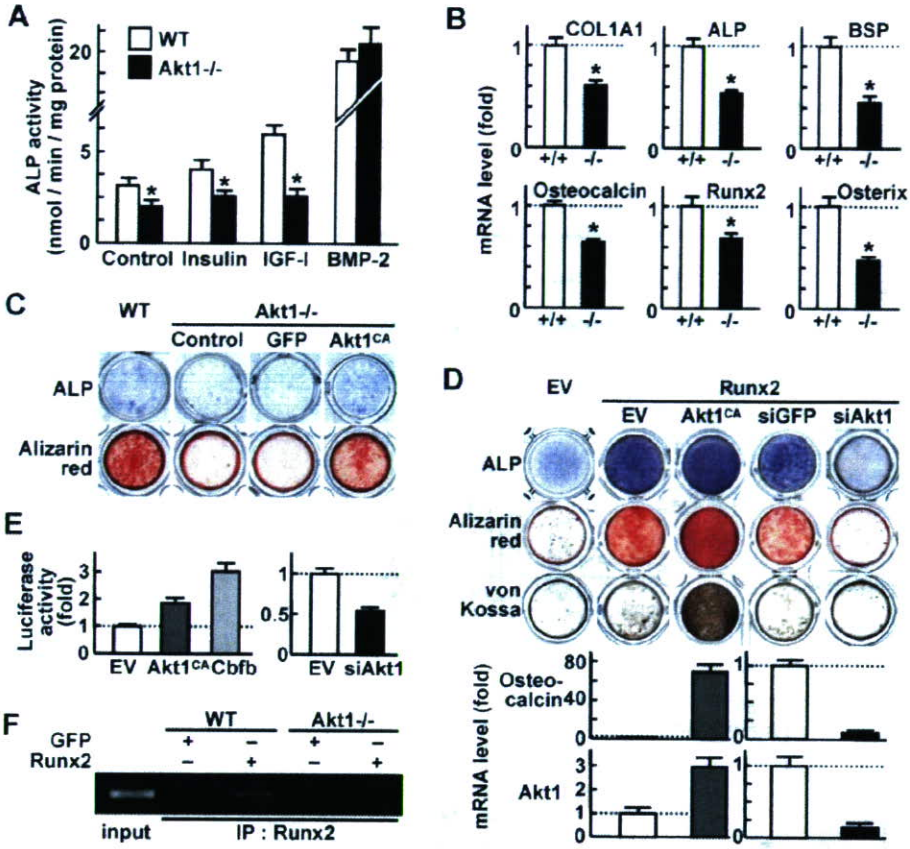

Figure 4. Akt1 enhances Runx2-dependent osteoblast differentiation and function. (A) ALP activity of WT and Akt1-/- osteoblasts cultured with and without insulin, IGF-I or BMP-2. Data are expressed as means (bars)±SEM (error bars) for 4 wells/group. *P<0.05 vs. WT. (B) mRNA levels of type I collagen (COL1A1), ALP, bone sialoprotein (BSP), osteocalcin, Runx2, and osterix in WT and Akt1-/- osteoblasts determined by real-time RT-PCR. Data are normalized to those of β-actin and are expressed as means (bars)±SEM (error bars) of the relative amount compared to WT culture. *P<0.01 vs. WT. (C) ALP and Alizarin red stainings of WT and Akt1-/- osteoblasts with and without adenoviral transfection of GFP or Akt1^{CA}. (D) ALP, Alizarin red, and von Kossa stainings of MC3T3-E1 cells retrovirally transfected with Runx2 or the empty vector (EV). Runx2 transfectants were retrovirally co-transfected with Akt1^{CA} or the control EV, and Akt1 siRNA (siAkt1) or the control (siGFP). The graphs indicate mRNA levels of osteocalcin and Akt1 determined by real-time RT-PCR. Data are normalized to those of β-actin and are expressed as means (bars)±SEM (error bars) of the relative amount compared to the control culture. (E) Osteocalcin promoter activity in retroviral Runx2 transfectants of MC3T3-E1 cells that were transfected with luciferase reporter constructs containing a 1,050 bp osteocalcin 5′-end flanking region. Plasmid vectors of Akt1^{CA}, the negative control EV, and the positive control Cbfb that is a representative co-activator of Runx2, as well as those of siAkt1 and the control EV were co-transfected. Data are expressed as means (bars)±SEM (error bars) of the fold change compared to EV. (F) ChIP assay using cell lysates of WT and Akt1-/- osteoblasts adenovirally transfected with GFP or Runx2. Purified DNA from with (IP) and without (input) immunoprecipitation by an antibody to Runx2 was amplified by PCR using a primer set in the mouse osteocalcin promoter region (−471/−67).
doi:10.1371/journal.pone.0001058.g004

introduction failed to commit immature mesenchymal cell lines C2C12 and C3H10T1/2 to osteoblastic lineage, although Runx2, a master transcription factor for osteoblastic differentiation, potently induced it (Supp. Fig S5).

These results suggest that Akt1 does not induce Runx2 expression but acts instead on differentiated osteoblasts that have the potency to express Runx2. Hence, as a possible mechanism underlying the osteogenic action of Akt1, we looked at its modulation of Runx2 function. Akt1 overexpression by Akt1^{CA} introduction into Runx2 stable transfectants of MC3T3-E1 cells enhanced the Runx2 activity on osteoblast differentiation and function, and vice versa, while Akt1 silencing by the siRNA introduction attenuated them (Fig 4D). Promoter activity of osteocalcin, a representative transcriptional target of Runx2, in Runx2-overexpressing MC3T3-E1 cells was also enhanced by Akt1^{CA} and suppressed by Akt1 siRNA (Fig 4E). Chromatin immunoprecipitation (ChIP) showed that the complex of Runx2 and osteocalcin promoter seen in WT osteoblasts disappeared in Akt1-/- osteoblasts (Fig 4F). Collectively, Akt1 is likely to enhance the Runx2-dependent osteoblast differentiation and function through enhancement of the DNA binding and the transcriptional activity.

Akt1 deficiency impairs bone resorption via dysfunctions of osteoclasts and osteoblasts

Finally, we investigated the role of Akt1 in bone resorption. The number of osteoclasts determined by tartrate-resistant acid phosphatase (TRAP) staining was reduced in the Akt1-/- bone in vivo (Fig 5A), which was confirmed by decreased bone

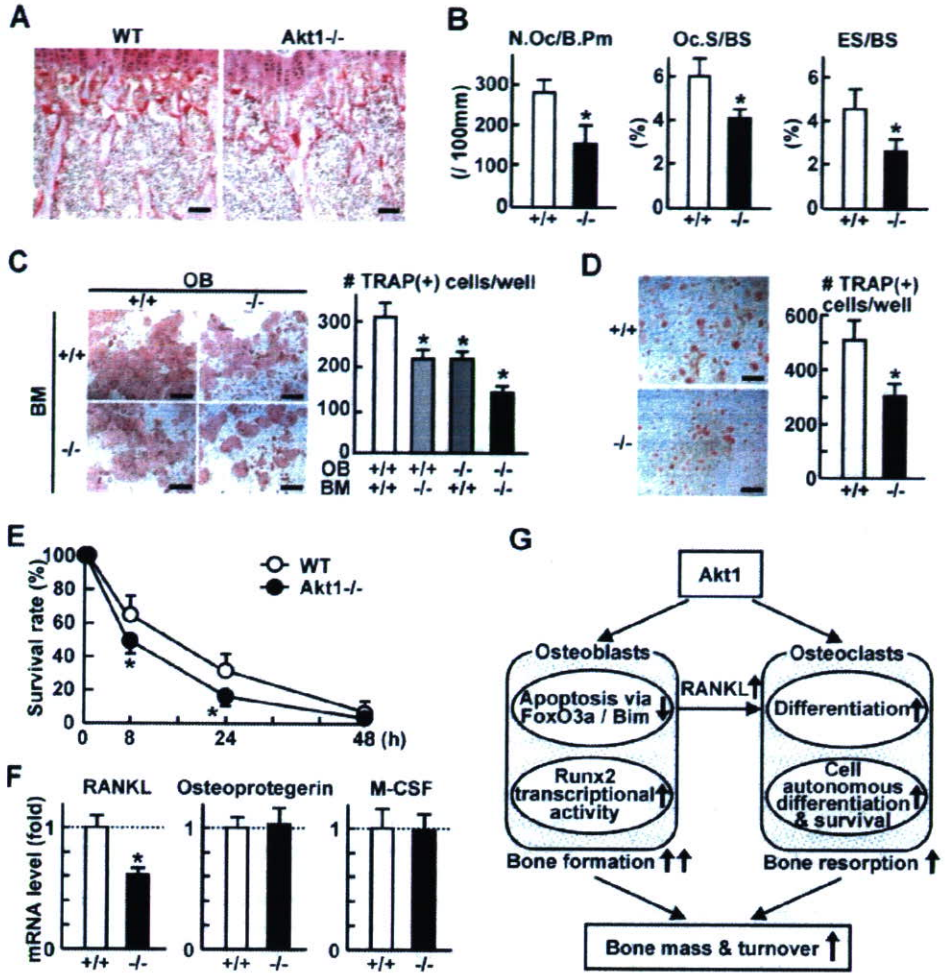

Figure 5. Akt1 deficiency impairs bone resorption via dysfunctions of osteoclasts and osteoblasts. (A) TRAP staining of proximal tibias of 8 week-old WT and Akt1-/- mice. Bars, 100 μm. (B) Bone resorption parameters in histomorphometric analysis at the secondary spongiosa of the proximal tibias. N.Oc/B. Pm, number of osteoclasts per 100 mm of bone perimeter; Oc.S/BS, osteoclast surface per bone surface; ES/BS, eroded surface per bone surface. Data are expressed as means (bars) ± SEM (error bars) for 3–4 mice/group. *P<0.05 vs. WT (+/+). (C) The number of TRAP-positive multinucleated osteoclasts formed in the coculture of osteoblasts (OB) and bone marrow cells (BM) from WT or Akt1-/- littermates. Data are expressed as means (bars) ± SEM (error bars) for 4 wells/group. *P<0.05 vs. WT. Bars, 500 μm. (D) The number of TRAP-positive multinucleated osteoclasts formed from BMM cultured in the presence of RANKL and M-CSF. Data are expressed as means (bars) ± SEM (error bars) for 4 wells/group. *P<0.01 vs. WT. Bars, 200 μm. (E) Time course of survival rate of mature osteoclasts after deprivation of RANKL and M-CSF. Mature osteoclasts were formed from BMM in the presence of RANKL and M-CSF. Data are expressed as means (symbols) ± SEM (error bars) for 4 wells/group. *P<0.05 vs. WT. (F) mRNA levels of RANKL, osteoprotegerin, and M-CSF in cultured osteoblasts by real-time RT-PCR. Data are normalized to those of β-actin and are expressed as means (bars) ± SEM (error bars) of the relative amount compared to the WT culture. *P<0.01 vs. WT. (G) Schematic diagram of the mechanisms underlying the Akt1 function to maintain bone mass and turnover. Akt1 suppresses the susceptibility to mitochondria-dependent apoptosis of osteoblasts by inhibiting the FoxO3a nuclear entry and the Bim transactivation, and stimulates the differentiation and function by enhancing the Runx2 transcriptional activity, resulting in increased bone formation. Akt1 also induces RANKL expression in osteoblasts to support osteoclast differentiation, and shows cell-autonomous defects in osteoclasts to stimulate the differentiation and survival, resulting in increased bone resorption.
doi:10.1371/journal.pone.0001058.g005

resorption parameters in the histomorphometric analysis (Fig 5B). Osteoclastogenesis in the ex vivo co-culture was reduced when either osteoblasts or bone marrow cells were derived from Akt1-/- mice, and was additively reduced when both were from Akt1-/- (Fig 5C). This indicates that Akt1 is necessary for osteoclast precursors in a cell autonomous manner and for osteoblasts to support osteoclast differentiation. Osteoclastogenesis in the culture of osteoclast-progenitor BMM derived from Akt1-/- was suppressed even in the presence of soluble receptor activator of nuclear factor κB ligand (RANKL) and M-CSF (Fig 5D). Furthermore, the survival of mature osteoclasts formed from Akt1-/- BMM was also impaired (Fig 5E), confirming that the intrinsic Akt1 in osteoclastic cells is necessary to maintain bone resorptive function. Contrarily, decreased expression of RANKL, but not osteoprotegerin or M-CSF, in Akt1-/- osteoblasts (Fig 5F) explains the contribution of Akt1 in osteoblasts to osteoclastic bone resorption.

Taken together, Akt1 deficiency may cause impairment of bone resorption via the cell autonomous dysfunction in osteoclasts and the cell non-autonomous inhibition of osteoclastogenesis due to reduced RANKL expression in osteoblasts.

DISCUSSION

Physiological roles of Akt1 in bone

The present study initially analyzed the bones of mice lacking Akt1 and found that the deficiency caused osteopenia with a low turnover state. Further in vivo and ex vivo analyses of osteoblasts and osteoclasts revealed that the Akt1 deficiency caused impairments of both bone formation and bone resorption via respective cell autonomous mechanisms (Fig 5G). The imbalance between formation and resorption, the underlying mechanism of which remains to be clarified, may cause osteopenia with a low bone turnover.

Akt1 in osteoblasts

Akt1 deficiency in osteoblasts caused three cell autonomous abnormalities: increased susceptibility to apoptosis, suppressed differentiation and function, and decreased RANKL expression to support osteoclastogenesis. Most notably among them, the enhanced apoptosis in Akt1-/- osteoblasts was shown to be mitochondria-dependent via the FoxO3a nuclear entry and the Bim transactivation. A recent report on mice with osteoblast-specific deletion of phosphatase and tensin homolog (Pten) demonstrated reduced osteoblast apoptosis and increased bone mass by constitutive activation of Akt signaling, corresponding to the present finding, although the downstream molecular mechanism remained unclarified [18]. The candidates of substrates of Akt1 included caspase-9, Bad, and FoxOs whose involvement in mitochondria-dependent apoptosis had been established in other cells [9]. Although caspase-9 functions as one of the most important effectors in the apoptosis, the lack of a minimal substrate consensus sequence for Akt [9] led us to exclude this from the candidates. A proapoptotic molecule Bad was expressed in osteoblasts, but the phosphorylation could not be detected. FoxO proteins identified in mammals, FoxO1, FoxO3a and FoxO4, constitute a newly characterized subfamily of the Forkhead/winged helix group of transcription factors and play a predominant role in mediating various functions of the PI3K/Akt pathway [16,17]. Although disruption of the genes in mice has revealed the necessities of FoxO1 in embryonic vessel formation and FoxO3a in ovarian follicular development [19], their roles in bone metabolism remained unknown. This study showed expressions of FoxO1 and FoxO3a, but not FoxO4, in osteoblasts, and functional involvement of FoxO3a in their survival as a phosphorylation target of Akt1. Contrarily, the nuclear entry of FoxO1 after serum deprivation was independent of Akt1 (Fig 2G), implicating that different isoforms of Akt may have specific preference to FoxO proteins as the substrates. In fact, similarly to Akt2, FoxO1 is expressed predominantly in insulin target tissues and regulates their insulin resistance [16].

Bim, Bcl-2-interacting mediator of cell death, was shown to be a transcriptional target of FoxO3a that lies downstream of the Akt1 anti-apoptotic signaling in osteoblasts. Proapoptotic activity of Bim is regulated both transcriptionally and post-transcriptionally [20], and the transcriptional induction is known to be mediated by FoxOs under the apoptotic stimulation in other cells [17,21–23]. Studies on knockout mice have revealed that Bim is essential for apoptosis of lymphocytes, myeloid cells, neurons, and osteoclasts [24,25]. Regarding osteoblast apoptosis, the involvement of Bcl-2 family proteins such as Bax and Bcl-2 has been reported [7,26]. Because the changes in protein levels of these molecules are crucial for osteoblast apoptosis, these changes seem to be independent of the Bim regulation.

Suppressed differentiation and function in Akt1-/- osteoblasts was shown to be mediated at least partly by modulating the Runx2 activity. The present results using Akt1-null materials confirmed a previous report by Fujita et al. that gain- and loss-of-functions of PI3K/Akt signaling regulate the DNA binding and transactivity of Runx2 in cultures of osteoblastic cells [27]. Since Runx2 does not have a consensus sequence for Akt phosphorylation, Akt is not likely to phosphorylate Runx2 directly, but may regulate the activity or stability of co-activators or co-repressors of Runx2. However, the fact that Akt1-/- mice did not exhibit cleidocranial dysplasia (Supp. Fig S2B), the characteristic phenotype of Runx2+/− mice, indicates that Akt1 is not a crucial regulator of the Runx2-dependent bone formation in vivo.

Akt1 in osteoclasts

Besides the defects in osteoblasts, the deficiency of Akt1 in osteoclasts caused impairment of bone resorption via the cell autonomous dysfunction. To date, the role of Akt signaling in osteoclasts has been controversial. RANKL and M-CSF have been reported to promote the osteoclast survival in part by activating the Akt pathway [28,29]. Contrarily, Akt is shown to be dispensable for the survival by knockdown experiment using Akt1/Akt2 siRNA, but is necessary for the proliferation and differentiation [30]. Our results using ex vivo cultures of isolated Akt1-/- osteoclasts have provided genetic evidence that Akt1 signaling promotes the differentiation and survival. The regulation of differentiation might be dependent on the DNA binding of NFκB, since previous knockdown studies of Akt1 and/or Akt2 showed inhibition of RANKL-induced NFκB p50 DNA-binding activity via IκB kinase α [30].

By analogy with osteoblasts, the enhanced osteoclast survival by Akt1 might be mediated by the FoxO3a/Bim axis, since Bim is reported to be critical for osteoclast apoptosis [25]. However, this is dependent on post-transcriptional regulation by ubiquitylation and proteasomal degradation of Bim mediated by ERK pathway, but not on transcriptional regulation as seen in the case of osteoblast apoptosis. In addition, Bim in osteoclasts stimulates not only the apoptosis, but also the bone resorptive activity. If Bim is enhanced in Akt1-/- osteoclasts just as in the osteoblasts, the bone resorption parameters like eroded surface are assumed to increase. Hence, the mechanism by which Akt1 suppresses apoptosis in osteoclasts is likely to be different from that in osteoblasts. The cell autonomous mechanism of Akt1 in osteoclasts is the next task we intend to pursue.

Akt1 as a mediator of bone anabolic signaling

Akt1 may mediate the osteoblastic bone formation by IGF-I and insulin, since their effects on osteoblast survival and differentiation were impaired in Akt1-/- osteoblasts (Fig 2C, 4A). Contrarily, although BMP-2 induced phosphorylation of the entire Akt (Supp. Fig S1A), the stimulated osteoblast differentiation was not affected by the Akt1 deficiency (Fig 4A), suggesting the mediation of other Akt isoforms or other pathways in the BMP-2 signaling. IGF-I is known to function as a potent bone anabolic factor via autocrine/paracrine and endocrine mechanisms [4], since skeletal and serum IGF-I levels were positively correlated with bone density between two inbred strains of mice [31]. Serum IGF-I levels of Akt1-/- mice were comparable to that of WT in the age from 8 to 16 weeks (data not shown), suggesting the absence of reduced IGF-I secretion or systemic compensation for impaired IGF-I signaling. Hence, the decreased bone formation in vivo in Akt1-/- mice may be at least in part due to the deficit of anabolic IGF-I signaling. Considering that Akt1; Akt2 double-knockout mice and IGF-I receptor knockout mice exhibit similar phenotypes [14,32], Akt may be the main mediator of the IGF-I signaling. Bone anabolic

action of other hormones like parathyroid hormone, growth hormone, and thyroid hormone are reported to be mediated by IGF-I signaling [33–36], and it is possible that the IGF-I/Akt1 pathway might be a common pathway for actions of these major hormones in bone.

As presented herein, Akt1, a multifaceted kinase which mediates various kinds of upstream signals to a diverse spectrum of substrates, plays multiple roles in bone cells as well as other cell types reported. Although it seems difficult to target this molecule directly in order to yield novel therapeutics for bone disorders because of its ubiquitous expression and diverse functions, further understanding of the molecular network related to Akt1 will greatly help us to unravel the complex mechanism modulating bone remodeling.

MATERIALS AND METHODS

Mice

The generation of Akt1-/- mice was described previously [11]. All mice were maintained in the C57BL/6 background with a standard diet. In each experiment, homozygous WT and Akt1-/- mice that were littermates generated from the intercross between heterozygous mice were compared. All experiments were performed on 8-week-old male mice unless otherwise described, according to the protocol approved by the Animal Care and Use Committee of the University of Tokyo.

Radiological analyses

Plain radiographs were taken using a soft X-ray apparatus (CMB-2, SOFTEX), and the BMD was measured by dual energy X-ray absorptiometry (DXA) using a bone mineral analyzer (PIXImus Densitometer, GE Medical Systems). CT scanning of the femurs was performed using a composite X-ray analyzer (NX-CP-C80H-IL, Nittetsu ELEX Co.), and reconstructed into a 3D feature by the volume-rending method (VIP-Station, Teijin System Technology). pQCT scan was performed at the metaphysis 1.4 mm above the distal growth plate and at the mid-shaft of femurs.

Histological analyses

For toluidine blue staining, samples were fixed with 70% ethanol, embedded in methyl methacrylate, and sectioned in 6-μm slices. Histomorphometric analyses were performed as described [37] in the growth plate and secondary spongiosa (1.2 mm in length from 0.5 mm below the growth plate) of the proximal tibias, according to the ASBMR nomenclature report [38]. For double labeling of the mineralization front, mice were injected subcutaneously with 16 mg/kg body weight of calcein at 5 d and 1 d before sacrifice. TRAP-positive cells were stained at pH 5.0 in the presence of L (+)-tartaric acid using naphthol AS-MX phosphate (Sigma-Aldrich) in *N,N*-dimethyl formamide as the substrate. Apoptotic osteoblasts were detected by TUNEL method using an ApopTag Peroxidase In Situ Apoptosis Detection Kit (Chemicon) on paraffin-embedded sections of neonate mice. The percentage of apoptotic cells was calculated by dividing the number of TUNEL-positive cells by the number of counted cells. A total of at least 400 osteoblasts were counted in each section, and five to seven sections per group were analyzed.

Osteoblastic cell cultures and assays

For osteoblast cultures, calvariae of neonatal mice were digested by 0.1% collagenase and 0.2% dispase 5 times, and cells isolated by the last 3 digestions were combined and cultured in α-minimal essential medium (α-MEM) containing 10% FBS. Mouse osteoblastic MC3T3-E1 cells were cultured in the same way. Immature mesenchymal C2C12 cells and C3H10T1/2 cells were cultured in Dulbecco's modified Eagle's medium (DMEM) supplemented with 10% FBS. Cell proliferation was determined using a BrdU Labeling and Detection Kit III (Roche Diagnostics). After 24 h culture in the presence and absence of insulin (100 nM), IGF-I (10 nM), or FGF-2 (1 nM), the cells were labeled with BrdU for an additional 4 h, and BrdU uptake was detected following the manufacturer's instructions. To determine the osteoblast apoptosis, the culture medium was changed to a serum-free one with and without insulin or IGF-I, and total RNA or protein was collected after designated times for subsequent assays. Cell survival was determined by counting viable cell numbers using the Cell Counting Kit-8 (Dojindo Molecular Technologies). Apoptotic osteoblasts were further detected by TUNEL staining as described above. Caspase-3 activity was measured via colorimetric detection of the cleavage of caspase-specific substrates using an APOPCYTO Caspase-3 Colorimetric Assay Kit (MBL International Co.). For ALP activity measurement, primary osteoblasts were inoculated at a density of 5×10^4 cells/well in a 24-multiwell plate and cultured in α-MEM containing 10% FBS and 50 μg/ml ascorbic acid. After 14 d of culture in the presence and absence of insulin (100 nM), IGF-I (10 nM), or BMP-2 (30 ng/ml), cells were sonicated in 10 mM Tris-HCl buffer (pH 8.0) containing 1 mM $MgCl_2$ and 0.5% Triton X-100. ALP activity in the lysate was measured using an ALP Kit (Wako Pure Chemical). Protein concentrations of cell lysates were measured with a Protein Assay Kit II (BIO-RAD). For ALP staining, cells were fixed in 70% ethanol and stained for 10 min with a solution containing 0.01% naphthol AS-MX phosphate, 1% *N,N*-dimethyl formamide, and 0.06% fast blue BB (Sigma-Aldrich). For Alizarin red S and von Kossa staining, osteoblasts were inoculated at a density of 1×10^5 cells/well in a 12-multiwell plate in α-MEM containing 10% FBS and 50 μg/ml ascorbic acid and 10 mM β-glycerophosphate (Sigma-Aldrich). On day 21 after confluency, cultured cells were fixed in 10% buffered formalin and stained for 10 min with 2% Alizarin red S (pH 4.0) (Sigma-Aldrich). For von Kossa staining, cells were fixed with 100% ethanol at room temperature for 15 min, stained with 5% silver nitrate solution under ultraviolet light for 10 min, and incubated for 5 min with 5% sodium thiosulfate solution.

Assays for osteoclastic cells

To study the role of Akt1 intrinsic to osteoclastic cells, we used a coculture of osteoblasts and bone marrow cells and the M-CSF-dependent BMM culture system as described previously [39]. Bone marrow cells were collected from long bones of 8-wk-old WT or Akt1-/- littermates. TRAP-positive multinucleated osteoclasts were generated by coculturing osteoblasts (1×10^4 cells/well) and bone marrow cells (5×10^5 cells/well) derived from either WT or Akt1-/- littermates in a 24-multiwell plate in α-MEM containing 10% FBS, $1,25(OH)_2D_3$ (10 nM), and prostaglandin E_2 (100 nM). After 6 d, cells positively stained for TRAP containing more than three nuclei were counted as osteoclasts. In the M-CSF-dependent BMM culture system, bone marrow cells from WT or Akt1-/- mice were seeded at a density of 3×10^5 cells/well in a 24-multiwell plate and cultured in α-MEM containing 10% FBS with M-CSF (R&D Systems, 100 ng/ml) for 3 d. To generate mature osteoclasts, adherent cells (BMM) were further cultured with M-CSF (10 ng/ml) and soluble RANKL (Wako Pure Chemical, 100 ng/ml) for 3 additional days, then the number of TRAP-positive osteoclasts was counted. To determine the survival, the mature osteoclasts were deprived of M-CSF/soluble RANKL and cultured for an additional 48 h. After 8, 24, and 48 h, the number